

Handling Multiplicity in Neuroimaging through Bayesian Lenses with Multilevel Modeling

Gang Chen^{*a}, Yaqiong Xiao^b, Paul A. Taylor^a, Justin K. Rajendra^a, Tracy Riggins^b, Fengji Geng^b,
Elizabeth Redcay^b, and Robert W. Cox^a

^aScientific and Statistical Computing Core, National Institute of Mental Health, USA

^bDepartment of Psychology, University of Maryland, USA

Abstract

Here we address the current issues of inefficiency and over-penalization in the massively univariate approach followed by the correction for multiple testing, and propose a more efficient model that pools and shares information among brain regions. Using Bayesian multilevel (BML) modeling, we control two types of error that are more relevant than the conventional false positive rate (FPR): incorrect sign (type S) and incorrect magnitude (type M). BML also aims to achieve two goals: 1) improving modeling efficiency by having one integrative model and thereby dissolving the multiple testing issue, and 2) turning the focus of conventional null hypothesis significant testing (NHST) on FPR into quality control by calibrating type S errors while maintaining a reasonable level of inference efficiency. The performance and validity of this approach are demonstrated through an application at the region of interest (ROI) level, with all the regions on an equal footing: unlike the current approaches under NHST, small regions are not disadvantaged simply because of their physical size. In addition, compared to the massively univariate approach, BML may simultaneously achieve increased spatial specificity and inference efficiency, and promote results reporting in totality and transparency. The benefits of BML are illustrated in performance and quality checking using an experimental dataset. The methodology also avoids the current practice of sharp and arbitrary thresholding in the p -value funnel to which the multidimensional data are reduced. The BML approach with its auxiliary tools is available as part of the AFNI suite for general use.

Introduction

The typical neuroimaging data analysis at the whole brain level starts with a preprocessing pipeline, and then the preprocessed data are fed into a voxel-wise time series regression model for each subject. An effect estimate is then obtained at each voxel as a regression coefficient that is, for example, associated with a task/condition or a contrast between two effects or a linear combination among multiple effects. Such effect estimates from individual subjects are next incorporated into a population model for generalization, which can be parametric (e.g., Student's t -test, AN(C)OVA, univariate (Poline and Brett, 2012) or multivariate GLM (Chen et al., 2014), linear mixed-effects (LME) (Chen et al., 2013)) or nonparametric (e.g., permutations (Nichols and Holmes, 2001; Smith and Nichols, 2009), bootstrapping, rank-based testing). In either case, this generally involves one or more statistical tests at each spatial element separately.

Issues with controlling false positives

As in many scientific fields, the typical neuroimaging analysis has traditionally been conducted under the framework of null hypothesis significance testing (NHST). As a consequence, a big challenge when presenting the population results is to properly handle the multiplicity issue resulting from the tens of thousands of simultaneous inferences, but this undertaking is met with various subtleties and pitfalls due to the complexities involved: the number of voxels in the brain (or a restricting mask) or the number of nodes on surface, spatial heterogeneity, violation of distributional assumptions, etc. The focus of

*Corresponding author. E-mail address: gangchen@mail.nih.gov

37 the present work will be on developing an efficient approach from Bayesian perspective to address the multiplicity issue as
38 well as some of the pitfalls associated with NHST (Appendix A). We first describe the multiplicity issue and how it directly
39 results from the NHST paradigm and inefficient modeling, and then translate many of the standard analysis features to
40 the proposed Bayesian framework.

41 Following the conventional statistical procedure, the assessment for a BOLD effect is put forward through a null
42 hypothesis H_0 as the devil’s advocate; for example, an H_0 can be formulated as having no activation at a brain region
43 under, for example, the easy condition, or as having no activation difference between the easy and difficult conditions. It is
44 under such a null setting that statistics such as Student’s t - or F -statistic are constructed, so that a standard distribution
45 can be utilized to compute a conditional probability that is the chance of obtaining a result equal to, or more extreme
46 than, the current outcome if H_0 is imagined as the ground truth. The rationale is that if this conditional probability is
47 small enough, one may feel comfortable in rejecting the straw man H_0 and in accepting the alternative at a tolerable risk.

48 While NHST may be a reasonable formulation under some scenarios, there is a long history of arguments that emphasize
49 the mechanical and interpretational problems with NHST (e.g., Cohen, 2014; Gelman, 2016) that might have perpetuated
50 the reproducibility crisis across many disciplines (Loken and Gelman, 2017). Within neuroimaging specifically, there are
51 strong indications that a large portion of task-related BOLD activations are usually unidentified at the individual subject
52 level due to the lack of power (Gonzalez-Castillo et al., 2012). The detection failure, or false negative rate, at the population
53 level would probably be at least as large. Therefore, it is likely far-fetched to claim that no activation or no activation
54 difference exists anywhere in the whole brain, except for the regions of white matter and cerebrospinal fluid. In other
55 words, the global null hypothesis in neuroimaging studies is virtually never true. The situation with resting-state data
56 analysis is likely worse than with task-related data, as the same level of noise is more impactful on seed-based correlation
57 analysis due to the lack of objective reference effect. Since no ground truth is readily available, dichotomous inferences
58 under NHST as to whether an effect exists in a brain region are intrinsically problematic, and it is practically implausible
59 to truly believe the validity of H_0 as a building block when constructing a model. Furthermore, the dichotomous filtering
60 under NHST paints a biased picture in the literature and leads to suboptimal meta analyses that are already compromised
61 without the incorporation or availability of effect reporting; for instance, conjunction analysis in neuroimaging is such an
62 artificial dichotomy of overlapping brain regions under two or more conditions based on arbitrary thresholding.

63 Achieving statistical significance has been widely used as the standard screening criterion in scientific results reporting
64 as well as in the publication reviewing process. The difficulty in passing a commonly accepted threshold with noisy data
65 may elicit a hidden misconception: A statistical result that survives the strict screening with a small sample size seems
66 to gain an extra layer of strong evidence, as evidenced by phrases in the literature such as “despite the small sample size”
67 or “despite limited statistical power.” However, when the statistical power is low, the inference risks can be perilous, as
68 demonstrated with two different types of error as illustrated in Appendix B from the conventional type I and type II
69 errors: incorrect sign (type S) and incorrect magnitude (type M). The conventional concept of FPR controllability is not
70 a well-balanced choice under all circumstances or combinations of effect and noise magnitudes. We consider a type S error
71 to be more severe than a type M error, and thus we aim to control the former while at the same time reducing the latter
72 as much as possible, parallel to the similarly lopsided strategy of strictly controlling type I errors at a tolerable level under
73 NHST while minimizing type II errors.

74 **Issues with handling multiplicity**

75 In statistics, multiplicity is more often referred to as multiple comparisons or multiple testing problem when more
76 than one statistical inference is made simultaneously. In neuroimaging, the multiplicity issue may sneak into data analysis
77 through several channels (Appendix C), affecting expected FPRs in diverse ways. One widely recognized aspect of multi-
78 plicity, multiple testing, occurs when the investigator fits [the same](#) model for each voxel in the brain. However, multiplicity
79 also occurs when the investigator conducts multiple comparisons within a model, tests two tails of a t -test separately
80 when prior information is unavailable about the directionality, and branches in the analytic pipelines. The challenges of
81 dealing with multiple testing at the voxel or node level have been recognized within the neuroimaging community almost
82 as long as the history of fMRI. Substantial efforts have been devoted to ensuring that the actual type I error (or FPR)
83 matches its nominal requested level under NHST. Due to the presence of spatial non-independence of noise, the classical
84 approach to countering multiple testing through Bonferroni correction in general is highly conservative when applied to
85 neuroimaging, so the typical correction efforts have been channeled into two main categories, 1) controlling for FWE, so
86 that the overall FPR at the cluster or whole brain level is approximately at the nominal value, and 2) controlling for false

87 discovery rate (FDR), which harnesses the expected proportion of identified items or discoveries that are incorrectly labeled
88 (Benjamini and Hochberg, 1995). FDR can be used to handle a needle-in-haystack problem where a small number of effects
89 existing among a sea of zero effects in, for example, bioinformatics. However, FDR is usually quite conservative for typical
90 neuroimaging data and thus is not widely adopted. Therefore, we do not discuss it hereafter in the current context.

91 Typical FWE correction methods for multiple testing include Monte Carlo simulations (Forman et al., 1995), random
92 field theory (Worsley et al., 1992), and permutation testing (Nichols and Holmes, 2001; Smith and Nichols, 2009). Re-
93 gardless of the specific FWE correction methodology, the common theme is to use the spatial extent, either explicitly or
94 implicitly, as a pivotal factor. One recent study suggested that the nonparametric methods seem to have achieved a more
95 uniformly accurate controllability for FWE than their parametric counterparts (Eklund et al., 2016), even though paramet-
96 ric methods may exhibit more flexibility in modeling capability (and some parametric methods can show reasonable FPR
97 controllability; Cox et al., 2017). Because of this recent close examination (Eklund et al., 2016) on the practical difficulties
98 of parametric approaches herein controlling FWE, there is currently an implied rule of thumb (e.g., Yeung, 2018) that
99 demands any parametric correction be based on a voxel-wise p -value threshold at 0.001 or less. Such a narrow modeling
100 choice with a harsh cutoff could be highly limiting, depending on several parameters such as trial duration (event-related
101 versus block design), and would definitely make small regions even more difficult to pass through the NHST filtering system.
102 In other words, the leverage on spatial extent with a Procrustean criterion undoubtedly incurs a collateral damage: small
103 regions (e.g., amygdala) or subregions within a brain area are inherently placed in a disadvantageous position even if small
104 regions have similar signal strength as larger ones; that is, to be able to surpass the same threshold bar, small regions
105 would have to reach a much higher signal strength to survive a uniform criterion at the cluster threshold or whole brain
106 level.

107 The concept of using contiguous spatial extent as a leveraging mechanism to control for multiplicity can be problematic
108 from another perspective. For example, suppose that two anatomically separate regions are spatially distant and the
109 statistical evidence (as well as signal strength) for each of their effects is not strong enough to pass the cluster correction
110 threshold individually. However, if another two anatomically regions that have exactly the same statistical evidence (as well
111 as signal strength) are adjacent, their spatial contiguity could elevate their combined volume to the survival of correction
112 for FWE. Trade-offs are inherently involved in these final interpretations. One may argue that the sacrifice in statistical
113 power under NHST is worth the cost in achieving the overall controllability of type I error, but it may be unnecessarily
114 over-penalizing to stick to such an inflexible criterion rather than utilizing the neurological context or prior knowledge, as
115 discussed below.

116 To summarize the debate surrounding cluster inferences, multiplicity is directly associated with the concept of false
117 positives or type I errors under NHST, and the typical control for FWE at a preset threshold (e.g., 0.05, the implicitly
118 accepted tolerance level in the field) is usually considered a safeguard for reproducibility. Imposing a threshold on cluster
119 size (perhaps combined with signal strength) to protect against the overall FPR has the undesirable trade-off cost of inflating
120 false negative rates or type II errors, which can greatly affect individual result interpretations as well as reproducibility
121 across studies. The current practice of handling multiple testing through controlling the overall FPR in neuroimaging under
122 the null hypothesis significance testing (NHST) paradigm excessively penalizes the statistical power with inflated type II
123 errors. More fundamentally, the adoption of dichotomous decisions through sharp thresholding under NHST may not be
124 appropriate when the null hypothesis itself is not pragmatically relevant because the effect of interest takes a continuum
125 instead of discrete values and is not expected to be null in most brain regions. When the noise inundates the signal,
126 two different types of error are more relevant than the concept of FPR: incorrect sign (type S) and incorrect magnitude
127 (type M). In general, several multiplicity-related challenges in neuroimaging appear to be tied closely to the fundamental
128 mechanisms of NHST approaches introduced to counterbalance between two counterfactual errors (type I and type II),
129 which are the cornerstones of NHST. Therefore, we put forward a list of potential problems with NHST in Appendix A.

130 **Structure of the work**

131 In light of the aforementioned backdrop, we believe that the current modeling approach is inefficient. First, we question
132 the appropriateness of the severe penalty currently levied to the voxel- or node-wise data analysis. In addition, we endorse
133 the ongoing statistical debate surrounding the ritualization of NHST and its dichotomous approach to results reporting and
134 in the review process, and aim to raise the awareness of the issues embedded within NHST (Loken and Gelman, 2017) in the
135 neuroimaging community. In addition, with the intention of addressing some of the issues discussed above, we view multiple
136 testing as a problem of inefficient modeling induced by the conventional massively univariate methodology. Specifically,

Table 1: Acronyms and terminology.

BML	Bayesian multilevel	NHST	null hypothesis significance testing
FPR	false positive rate	NUTS	No-U-Turn sampler
FWE	family-wise error	power	chance of rejecting H_0 when H_0 is false
GLM	general linear model	PPC	posterior predictive check
HMC	Hamiltonian Monte Carlo	type I	chance of rejecting H_0 when H_0 is true (“false positive”)
LME	linear mixed-effects	type II	failing to reject H_0 when H_0 is false (“false negative”)
LOO	leave one out	type M	exaggerating the effect magnitude
MCMC	Markov chain Monte Carlo	type S	estimating the effect with an incorrect sign

137 the univariate approach starts, in the same vein as a null hypothesis setting, with a pretense of spatial independence, and
138 proceeds with many isolated or segmented models. To avoid the severe penalty of Bonferroni correction while recovering
139 from or compensating for the false presumption of spatial independence, the current practices deal with multiple testing by
140 discounting the number of models due to spatial relatedness. However, the collateral damages incurred by this to-and-fro
141 process are unavoidably the loss of modeling efficiency and the penalty for detection power under NHST.

142 Here, we propose a more efficient approach through BML that could be used to confirm, complement or replace the
143 standard NHST method. As a first step, we adopt a group analysis strategy under the Bayesian framework through
144 multilevel modeling on an ensemble of ROIs and use this to resolve two of the four multiplicity issues above: multiple
145 testing and double sidedness (Appendix C). Those ROIs are determined independently from the current data at hand, and
146 they can be selected through various methods such as previous studies, an anatomical or functional atlas, or parcellation
147 of an independent dataset in a given study; the regions could be defined through masking, manual drawing, or balls about
148 a center reported previously. The proposed BML approach dissolves multiple testing through a multilevel model that more
149 accurately accounts for data structure as well as shared information, and it consequentially improves inference efficiency.
150 The modeling approach will be extended to other scenarios in our future work.

151 As a novel approach, BML here is applied to neuroimaging in dealing with multiplicity at the ROI level, with a potential
152 extension to whole brain analysis in future work. We present this work in a purposefully (possibly overly) didactic style in
153 the appendices, reflecting our own conceptual progression. Our goal is to convert the traditional voxel-wise GLM into an
154 ROI-based BML through a step-wise progression of models (GLM \rightarrow LME \rightarrow BML). The paper is structured as follows.
155 In the next section, we first formulate the population analysis at each ROI through univariate GLM (parallel to the typical
156 voxel-wise population analysis), then turn multiple GLMs into one LME by pivoting the ROIs as the levels of a random-
157 effects factor¹, and lastly convert the LME to a full BML. The BML framework does not make statistical inferences
158 for each measuring entity (ROI in our context) in isolation. Instead, the BML weights and borrows the information
159 based on the precision information across the full set of entities, striking a balance between data and prior knowledge; in a
160 nutshell, the crucial feature here is that the ROIs, instead of being loose, are associated with each other through a Gaussian
161 assumption under BML. As a practical exemplar, we apply the modeling approach to an experimental dataset and compare
162 its performance with the conventional univariate GLM. In the Discussion section, we elaborate the advantages, limitations,
163 and prospects of BML in neuroimaging. Major acronyms and terms are listed in Table 1.

164 Theory: Bayesian multilevel modeling

165 Throughout this article, the word *effect* refers to a quantity of interest, usually embodied in a regression (or correlation)
166 coefficient, the contrast between two such quantities, or the linear combination of two or more such quantities from individual
167 subject analysis. Italic letters in lower case (e.g., α) stand for scalars and random variables; lowercase, boldfaced italic
168 letters (\mathbf{a}) for column vectors; Roman and Greek letters for fixed and random effects in the conventional statistics context,
169 respectively, on the righthand side of a model equation (the Greek letter θ is reserved for the effect of interest); $p(\cdot)$
170 represents a probability density function.

¹In real practice, the ROIs are not randomly drawn from a hypothetical pool like recruiting experimental subjects. However, from the practical perspective it is not too far-fetched to assume that the effects at those ROIs form a distribution such as Gaussian, similar to the assumption of Gaussian distribution for cross-subject effects. It is under this assumption that we treat the cross-ROI effects as random, and the assumption can be further validated through various cross-validation methods and model comparisons later in this paper.

As our main focus here is fMRI population analysis, we extend the BML approach for one-way ANOVA (Appendix D) to a two-way ANOVA structure, and elucidate the advantages of data calibration and partial pooling in more details. At the population level, the variability across n subjects has to be accounted for; in addition, the within-subject correlation structure among the ROIs also needs to be maintained. The conventional approach formulates r separate GLMs each of which fits the data y_{ij} from the i th subject at the j th ROI,

$$y_{ij} = \theta_j + \epsilon_{ij}, \quad i = 1, 2, \dots, n, \quad (1)$$

where $j = 1, 2, \dots, r$, θ_j is the population effect at the j th ROI, and ϵ_{ij} is the residual term that is assumed to independently and identically follow $\mathcal{N}(0, \sigma^2)$. Each of the r models in (1) essentially corresponds to a Student's t -test, and the immediate challenge is the multiple testing issue among those r models: with the assumption of exchangeability among the ROIs, is Bonferroni correction the only valid solution? If so, most neuroimaging studies would have difficulty in adopting ROI-based analysis due to this severe penalty, which may be the major reason that discourages the use of region-level analysis with a large number of regions. Alternatively, the r separate GLMs in (1) can be merged into one GLM by pooling the variances across the r ROIs,

$$y_{ij} = \theta_j + \epsilon_{ij}, \quad i = 1, 2, \dots, n, j = 1, 2, \dots, r. \quad (2)$$

The two approaches, (1) and (2), usually render similar inferences unless the sampling variances are dramatically different across the ROIs. To compare different models through information criteria (Vehtari et al., 2017), we can solve the GLM (2) in a Bayesian fashion,

$$y_{ij} | \theta_j \sim \mathcal{N}(\theta_j, \sigma^2), \quad i = 1, 2, \dots, n, \quad j = 1, 2, \dots, r, \quad (3)$$

where the effects θ_j are assigned with a noninformative prior so that no pooling is applied among the ROIs, leading to virtually identical inferences as the GLM (2).

The approach with model (1), (2), or (3) does not involve any pooling among the ROIs in the sense that the information at one ROI is assumed to reveal nothing about any other ROIs, and may lead to overfitting. To improve model fitting, we first adopt two-way random-effects ANOVA, and formulate the following platform with data from n subjects,

$$y_{ij} = b_0 + \pi_i + \xi_j + \epsilon_{ij}, \quad i = 1, 2, \dots, n, \quad j = 1, 2, \dots, r, \quad (4)$$

where b_0 represents the population effect, π_i and ξ_j code the deviation or random effect of the i th subject and j th ROI from the overall mean b_0 , respectively, and they are assumed to be *iid* with² $\mathcal{N}(0, \lambda^2)$ and $\mathcal{N}(0, \tau^2)$, and ϵ_{ij} is the residual term that is assumed to follow $\mathcal{N}(0, \sigma^2)$.

Parallel to the situation with one-way ANOVA (Appendix D), the two-way ANOVA (4) can be conceptualized as an LME without changing its formulation. Specifically, the overall mean b_0 is a fixed-effects parameter, while both the subject- and ROI-specific effects, π_i and ξ_j , are treated as random variables. When $n, r \geq 3$, the number of data points nr is greater than the total number of model parameters, $n + r + 2$, both the ANOVA and LME frameworks are identifiable. In addition, we continue to define $\theta_j = b_0 + \xi_j$ as the effect of interest at the j th ROI. The LME framework has been well developed over the past half century, under which we can estimate variance components such as λ^2 and τ^2 , and fixed effects such as b_0 in (4). Therefore, conventional inferences can be made by constructing an appropriate statistic for a null hypothesis. Its modeling applicability and flexibility have been substantiated by its adoption in fMRI group analysis (Chen et al., 2013). Furthermore, the LME formulation (4) has a special layout, a crossed random-effects (or cross-classified) structure, which has been applied to inter-subject correlation (ISC) analysis for naturalistic scanning (Chen et al., 2017a) and to ICC analysis for ICC(2,1) (Chen et al., 2017c). A hierarchical model is a particular multilevel model in which parameters are nested within one another, and the cross-classified structure here showcases the difference between the two conceptions: the two clusters (ROI and subjects) intertwine with each other and form a factorial structure (n subjects by r ROIs), distinct from a hierarchical or nested one.

²For simplicity, here we assume that both π_i and ξ_j being independent and identically distributed (*iid*). In reality, the strict *iid* assumption can be problematic for the cross-ROI effects when they are spatially proximate or neurologically related. Nevertheless, the assumption can be relaxed later on to exchangeability for BML.

However, LME cannot offer a solution in making inferences regarding the ROI effects θ_j : to estimate θ_j , the LME (4) would become over-parameterized (i.e., an over-fitting problem). To proceed for the sake of intuitive interpretations, we temporarily assume a known sampling variance σ^2 , a known cross-subjects variance λ^2 , and a known cross-ROI variance τ^2 , and transform the ANOVA (4) to its Bayesian counterpart,

$$y_{ij}|\pi_i, \theta_j \sim \mathcal{N}(\pi_i + \theta_j, \sigma^2), \quad i = 1, 2, \dots, n, \quad j = 1, 2, \dots, r. \quad (5)$$

Then the posterior distribution of θ_j with prior distributions, $\pi_i \sim \mathcal{N}(0, \lambda^2)$ and $\theta_j \sim \mathcal{N}(b_0, \tau^2)$, can be analytically derived (Appendix E) with the data $\mathbf{y} = \{y_{ij}\}$,

$$\theta_j|b_0, \tau, \lambda, \mathbf{y} \sim \mathcal{N}(\hat{\theta}_j, V), \quad \text{where } \hat{\theta}_j = \frac{\frac{n}{\lambda^2 + \sigma^2} \bar{y}_{\cdot j} + \frac{1}{\tau^2} b_0}{\frac{n}{\lambda^2 + \sigma^2} + \frac{1}{\tau^2}}, \quad V = \frac{1}{\frac{n}{\lambda^2 + \sigma^2} + \frac{1}{\tau^2}}, \quad j = 1, 2, \dots, r. \quad (6)$$

Similarly to the one-way ANOVA scenario (Appendix D), we have an intuitive interpretation for $\frac{1}{V} = \frac{n}{\lambda^2 + \sigma^2} + \frac{1}{\tau^2}$: the posterior precision for $\theta_j|b_0, \tau, \lambda, \mathbf{y}$ is the sum of the cross-ROI precision $\frac{1}{\tau^2}$ and the combined sampling precision $\frac{n}{\lambda^2 + \sigma^2}$. Under the r completely separate GLMs in (1), the cross-subjects variance λ^2 and the sampling variance σ^2 could not be estimated separately. Interestingly, the following relationship,

$$\frac{n}{\lambda^2 + \sigma^2} < \frac{1}{V} = \frac{n}{\lambda^2 + \sigma^2} + \frac{1}{\tau^2} \leq \frac{n}{\sigma^2} + \frac{1}{\tau^2}, \quad (7)$$

reveals that the posterior precision lies somewhere among the precisions of $\hat{\theta}_j$ from the r separate GLMs. Furthermore, the posterior mode of $\hat{\theta}_j$ in (6) can be expressed as a weighted average between the individual sample means $\bar{y}_{\cdot j}$ and the overall mean b_0 ,

$$\hat{\theta}_j = \frac{\frac{n}{\lambda^2 + \sigma^2} \bar{y}_{\cdot j} + \frac{1}{\tau^2} b_0}{\frac{n}{\lambda^2 + \sigma^2} + \frac{1}{\tau^2}} = w \bar{y}_{\cdot j} + (1 - w) b_0 = b_0 + w(\bar{y}_{\cdot j} - b_0) = \bar{y}_{\cdot j} - (1 - w)(\bar{y}_{\cdot j} - b_0), \quad j = 1, 2, \dots, r, \quad (8)$$

191 where the weight $w = \frac{nV}{\lambda^2 + \sigma^2}$, indicating the counterbalance of partial pooling between the individual mean $\bar{y}_{\cdot j}$ for the
 192 j th entity and the overall mean b_0 , the adjustment of θ_j from the overall mean b_0 toward the observed mean $\bar{y}_{\cdot j}$, or the
 193 observed mean $\bar{y}_{\cdot j}$ being shrunk toward the overall mean b_0 .

Related to the concept of ICC, the correlation between two ROIs, j_1 and j_2 , due to the fact that they are measured from the same set of subjects, can be derived in a Bayesian fashion as,

$$\begin{aligned} \text{corr}(y_{ij_1}, y_{ij_2} | \lambda^2, \tau^2, \sigma^2) &= \frac{\text{cov}(\pi_i + \theta_{j_1} + \epsilon_{ij_1}, \pi_i + \theta_{j_2} + \epsilon_{ij_2})}{\sqrt{\text{var}(\pi_i + \theta_{j_1} + \epsilon_{ij_1}) \text{var}(\pi_i + \theta_{j_2} + \epsilon_{ij_2})}} | \lambda^2, \tau^2, \sigma^2 \\ &= \frac{\lambda^2}{\lambda^2 + \tau^2 + \sigma^2}, \quad j_1, j_2 = 1, 2, \dots, r \quad (j_1 \neq j_2). \end{aligned} \quad (9)$$

Similarly, the correlation between two subjects, i_1 and i_2 , due to the fact that their effects are measured from the same set of ROIs, can be derived in a Bayesian fashion as,

$$\begin{aligned} \text{corr}(y_{i_1 j}, y_{i_2 j} | \lambda^2, \tau^2, \sigma^2) &= \frac{\text{cov}(\pi_{i_1} + \theta_j + \epsilon_{i_1 j}, \pi_{i_2} + \theta_j + \epsilon_{i_2 j})}{\sqrt{\text{var}(\pi_{i_1} + \theta_j + \epsilon_{i_1 j}) \text{var}(\pi_{i_2} + \theta_j + \epsilon_{i_2 j})}} | \lambda^2, \tau^2, \sigma^2 \\ &= \frac{\tau^2}{\lambda^2 + \tau^2 + \sigma^2}, \quad i_1, i_2 = 1, 2, \dots, n \quad (i_1 \neq i_2). \end{aligned}$$

194 The exchangeability assumption is crucial here as well for the BML system (4). Conditional on ξ_j (i.e., when the ROI
 195 is fixed at index j), the subject effects π_i can be reasonably assumed to be exchangeable since the experiment participants
 196 are usually recruited randomly from a hypothetical population pool as representatives (thus the concept of coding them
 197 as dummy variables). As for the ROI effects ξ_j , here we simply assume the validity of exchangeability conditional on the
 198 subject effect π_i (i.e., when subject is fixed at index i), and address the validity later in Discussion.

199 To summarize, the main difference between the conventional GLM and BML lies in the assumption about the brain
 200 regions: the effects (e.g., θ_j in (3)) are assumed to have a noninformative flat prior while they are assigned with a Gaussian
 201 prior under BML. In other words, the effect at each region is estimated independently from other regions under GLM, thus
 202 there is no information shared across regions. In contrast, the effects across regions are shared, regularized and partially
 203 pooled through the Gaussian assumption under BML for the effects across regions; such a cross-region Gaussian assumption

204 bears the same rationale as the cross-subject Gaussian assumption. So far, we have presented a “simplest” BML scenario.
 205 Specifically, we have: ignored the possibility of incorporating any explanatory variables such as subject-specific quantities
 206 (e.g., age, IQ) or behavioral data (e.g., reaction time); assumed known variances such as τ^2 and σ^2 ; and presumed that the
 207 data y_{ij} have been directly measured without precision information available. Further extensions are needed and discussed
 208 for realistic applications in the next subsection.

209 Further extensions of Bayesian modeling for two-way random-effects ANOVA and full 210 Bayesian implementations

211 To gain intuitive interpretations, we have so far assumed that the variances σ^2 , λ^2 and τ^2 in (5) (and σ^2 in (23)
 212 of Appendix D) are known. In practice, those parameters for the prior distributions are not available. Approximate
 213 (or empirical) Bayesian approaches could be adopted to provide a computationally economical “workaround” solution.
 214 For example, one possibility is to first solve the corresponding LME and directly apply the estimated variances to the
 215 analytical formula (6) (and (24) in Appendix D). However, there are two limitations associated with approximate Bayesian
 216 approaches. The reliability or uncertainty for the estimated variances are not taken into consideration and thus may result
 217 in inaccurate posterior distributions. In addition, analytical formulas such as (6) (and (24) in Appendix D) are usually
 218 not available when we extend the prototypical models (5) (and (23) in Appendix D) to more generic scenarios, as shown
 219 below.

At the population level, one may incorporate one or more subject-specific covariates such as subject-grouping variables
 (patients vs. controls, genotypes, adolescents vs. adults), within-subject (e.g., multiple conditions such as positive, negative
 and neutral emotions) or quantitative explanatory variables (age, behavioral or biometric data). To be able to adapt such
 scenarios, we first need to expand the models considered previously with a simple intercept (Student’s t -test) to r separate
 GLMs and one GLM with pooled variances, generalizing the models (1) and (3), respectively, to

$$y_{ij} = \mathbf{x}_i^T \boldsymbol{\theta}_j + \epsilon_{ij}, \quad i = 1, 2, \dots, n, \quad (10)$$

$$y_{ij} | \boldsymbol{\theta}_j \sim \mathcal{N}(\mathbf{x}_i^T \boldsymbol{\theta}_j, \sigma^2), \quad i = 1, 2, \dots, n, \quad j = 1, 2, \dots, r, \quad (11)$$

where the vector \mathbf{x}_i contains the subject-specific values of the covariates, with its first component 1 that is associated with
 the intercept, and the vector $\boldsymbol{\theta}_j$ codes the effects associated with the covariates \mathbf{x}_i (and each component in $\boldsymbol{\theta}_j$ is assigned
 with a noninformative prior in (11)), $j = 1, 2, \dots, r$. In parallel, the conventional two-way random-effects ANOVA or LME
 (4) evolves to

$$y_{ij} = \mathbf{x}_i^T \mathbf{b} + \pi_i + \mathbf{x}_i^T \boldsymbol{\xi}_j + \epsilon_{ij}, \quad i = 1, 2, \dots, n, \quad j = 1, 2, \dots, r, \quad (12)$$

where \mathbf{b} and $\boldsymbol{\xi}_j$ represent the population effects and region-specific deviations corresponding to those covariates, respectively.
 Similarly, the BML counterpart can be formulated as

$$y_{ij} | \mathbf{x}_i, \mathbf{b}, \pi_i, \boldsymbol{\xi}_j \sim \mathcal{N}(\mathbf{x}_i^T \mathbf{b} + \pi_i + \mathbf{x}_i^T \boldsymbol{\xi}_j, \sigma^2), \pi_i \sim \mathcal{N}(0, \lambda^2), \boldsymbol{\xi}_j \sim \mathcal{N}(\mathbf{0}, \boldsymbol{\tau}), \quad i = 1, 2, \dots, n, \quad j = 1, 2, \dots, r, \quad (13)$$

220 where $\boldsymbol{\tau}$ is a 2×2 variance-covariance matrix for $\boldsymbol{\xi}_j$.

Under the BML (13), the effect of interest θ_j can be an element of \mathbf{b} , the intercept (as in (5)) or the effect for one of
 the covariates \mathbf{x}_i . Similar to models with varying intercepts such as (4) and (5), both intercepts and slopes are assumed
 to be different across ROIs in the models (12) and (13), and they are usually referred to as models with varying intercepts
 and slopes. When there is only one covariate x_i , the four models (10), (11), (12) and (13) simplify to, respectively,

$$y_{ij} = \theta_{0j} + \theta_{1j} x_i + \epsilon_{ij}, \quad i = 1, 2, \dots, n, \quad (14)$$

$$y_{ij} | x_i, \theta_{0j}, \theta_{1j} \sim \mathcal{N}(\theta_{0j} + \theta_{1j} x_i, \sigma^2), \quad i = 1, 2, \dots, n, \quad j = 1, 2, \dots, r, \quad (15)$$

$$y_{ij} = b_0 + b_1 x_i + \pi_i + \xi_{0j} + \xi_{1j} x_i + \epsilon_{ij}, \quad i = 1, 2, \dots, n, \quad j = 1, 2, \dots, r, \quad (16)$$

$$y_{ij} | x_i, b_0, b_1, \pi_i, \xi_{0j}, \xi_{1j} \sim \mathcal{N}(b_0 + b_1 x_i + \pi_i + \xi_{0j} + \xi_{1j} x_i, \sigma^2), \quad \pi_i \sim \mathcal{N}(0, \lambda^2), \quad (\xi_{0j}, \xi_{1j})^T \sim \mathcal{N}((0, 0)^T, \boldsymbol{\tau}) \quad (17)$$

$$i = 1, 2, \dots, n, \quad j = 1, 2, \dots, r,$$

221 where $\boldsymbol{\tau}$ is a 2×2 variance-covariance matrix for $(\xi_{0j}, \xi_{1j})^T$.

222 The discussion so far has assumed that data y_{ij} are directly collected without measurement errors. However, in some
223 circumstances (including neuroimaging) the data are summarized through one or more analytical steps. For example, the
224 data y_{ij} in fMRI can be the BOLD responses from subjects under a condition or task that are estimated through a time
225 series regression model, and the estimates are not necessarily equally reliable. Therefore, a third extension is desirable to
226 broaden our model (13) so that we can accommodate the situation where the separate variances σ_{ij}^2 of measurement errors
227 for each ROI and subject are known and should be included in the model (13) as inputs, instead of being treated as one
228 hyperparameter. Similarly to the conventional meta-analysis, a BML with known sampling variances can be effectively
229 analyzed by simply treating the variances as known values.

230 Numerical implementations of BML

231 Since no analytical formula is generally available for the BML (13), we proceed with the full Bayesian approach hereafter,
232 and adopt the algorithms implemented in Stan, a probabilistic programming language and a math library in C++ on which
233 the language depends (Stan Development Team, 2017). In Stan, the main engine for Bayesian inferences is No-U-Turn
234 sampler (NUTS), a variant of Hamiltonian Monte Carlo (HMC) under the category of gradient-based Markov chain Monte
235 Carlo (MCMC) algorithms.

236 Some conceptual and terminological clarifications are warranted here. Under the LME framework, the differentiation
237 between fixed- and random-effects is clearcut: fixed-effects parameters (e.g., \mathbf{b} in (12)) are considered universal constants
238 at the population level to be estimated; in contrast, random-effects variables (e.g., π_i and $\boldsymbol{\xi}_j$ in (12)) are assumed to be
239 varying and follow a presumed distribution. However, there is no such distinction between fixed and random effects in
240 Bayesian formulations, and all effects are treated as parameters and are assumed to have prior distributions. Nevertheless,
241 there is a loose correspondence between LME and BML: fixed effects under LME are usually termed as population effects
242 under BML, while random effects in LME are typically referred to as entity effects³ under BML.

243 Essentially, the full Bayesian approach for the BML systems (5) and (13) can be conceptualized as assigning hyperpriors
244 to the parameters in the LME or ANOVA counterparts (4), and (12). Our hyperprior distribution choices follow the
245 general recommendations in Stan (Stan Development Team, 2017). Specifically, an improper flat (noninformative uniform)
246 distribution over the real domain for the population parameters (e.g., \mathbf{b} in (13)) is adopted, since we usually can afford
247 the vagueness thanks to the usually satisfactory amount of information available in the data at the population level. For
248 the scaling parameters at the entity level, the variances for the cross-subjects effects π_i and as well as in the variance-
249 covariance matrix for $\boldsymbol{\xi}_j$ in (13), we use a weakly informative prior such as a Student’s half- $t(3, 0, 1)$ ⁴ or half-Gaussian
250 $\mathcal{N}(0, 1)$ (restricting to the positive half of the respective distribution). For the covariance structure of $\boldsymbol{\xi}_j$, the LKJ correlation
251 prior⁵ is used with the parameter $\zeta = 1$ (i.e., jointly uniform over all correlation matrices of the respective dimension).
252 Lastly, the variance for the residuals ϵ_{ij} is assigned with a half Cauchy prior with a scale parameter depending on the
253 standard deviation of y_{ij} .

254 To summarize, besides the Bayesian framework under which hyperpriors provide a computational convenience through
255 numerical regularization, the major difference between BML and its univariate GLM counterpart is the Gaussian assumption
256 for the ROIs (e.g., $\theta_j \sim \mathcal{N}(b_0, \tau^2)$ in the model (5)) that plays the pivotal role of pooling and sharing the information
257 among the brain regions. It is this partial pooling that effectively takes advantage of the effect similarities among the
258 ROIs and achieves higher modeling efficiency. **In other words, we dissolve the multiple testing issue through borrowing
259 information across the ROIs by incorporating the regions into one model with a prior assumption about their effects. In
260 contrast, the inefficiency of the massively univariate approach lies in the fact that the modeler pretends that each voxel or
261 ROI is unrelated and would have to pay the penalty for the pretense.**

262 Another different aspect about Bayesian inference is that it hinges around the whole posterior distribution of an
263 effect. For practical considerations in results reporting, modes such as mean and median are typically used to show the
264 centrality, while a quantile-based (e.g., 95%) interval or highest posterior density provides a condensed and practically
265 useful summary of the posterior distribution. The typical workflow to obtain the posterior distribution for an effect of

³Entity effects are more popularly called group effects in the Bayesian literature. However, to avoid potential confusions with the neuroimaging terminology in which the word *group* refers to subject categorization (e.g., males vs. females, patients vs. controls) or the analytical step of generalization from individual subjects to the group (corresponding to the word *population* in the Bayesian literature) level, we adopt *entity* to mean each measuring unit such as subject and ROI in the current context.

⁴See https://en.wikipedia.org/wiki/Folded-t_and_half-t_distributions for the density $p(\nu, \mu, \sigma^2)$ of folded non-standardized t -distribution, where the parameters ν , μ , and σ^2 are the degrees of freedom, mean, and variance.

⁵The LKJ prior (Lewandowski, Kurowicka, and Joe, 2009) is a distribution over symmetric positive-definite matrices with the diagonals of 1s.

266 interest is the following. Multiple (e.g., 4) Markov chains are usually run in parallel with each of them going through a
 267 predetermined number (e.g., 2000) of iterations, half of which are thrown away as warm-up (or “burn-in”) iterations while
 268 the rest are used as random draws from which posterior distributions are derived. To gauge the consistency of an ensemble
 269 of Markov chains, the split \hat{R} statistic (Gelman et al., 2014) is provided as a potential scale reduction factor on split chains
 270 and as a diagnostic parameter to assist the analyst in assessing the quality of the chains. Ideally, fully converged chains
 271 correspond to $\hat{R} = 1.0$, but in practice $\hat{R} < 1.1$ is considered acceptable. Another useful parameter, the number of effective
 272 sampling draws after warm-up, measures the number of independent draws from the posterior distribution that would be
 273 expected to produce the same standard deviation of the posterior distribution as is calculated from the dependent draws
 274 from HMC. As the sampling draws are not always independent with each other, especially when Markov chains proceed
 275 slowly, one should make sure that the effective sample size is large enough relative to the total sampling draws so that a
 276 reasonable accuracy can be achieved to derive the quantile intervals for the posterior distribution. For example, a 95%
 277 quantile interval requires at least an effective sample size of 100. As computing parallelization can only be executed for
 278 multiple chains of the HMC algorithms, the typical BML analysis can be effectively conducted on any system with at least
 279 4 CPUs.

280 One important aspect of the Bayesian framework is model quality check through various prediction accuracy metrics.
 281 The aim of the quality check is not to reject the model, but rather to check whether it fits the data well. For instance,
 282 posterior predictive check (PPC) simulates replicated data under the fitted model and then graphically compares actual data
 283 y_{ij} to the model prediction. The underlying rationale is that, through drawing from the posterior predictive distribution,
 284 a reasonable model should generate new data that look similar to the acquired data at hand. As a model validation tool,
 285 PPC intuitively provides a visual tool to examine any systematic differences and potential misfit of the model, similar to
 286 the visual examination of plotting a fitted regression model against the original data. Leave-one-out (LOO) cross-validation
 287 using Pareto-smoothed importance sampling (PSIS) is another accuracy tool (Vehtari et al., 2017) that uses probability
 288 integral transformation (PIT) checks through a quantile-quantile (Q-Q) plot to compare the LOO-PITs to the standard
 289 uniform or Gaussian distribution.

290 BML applied to an ROI-based group analysis

291 To demonstrate the performances of BML in comparison to the conventional univariate approach at the ROI level,
 292 we utilized an experimental dataset from a previous fMRI study (Xiao et al., 2018). Briefly, a cohort of 124 typically
 293 developing children (mean age = 6.6 years, SD = 1.4 years, range = 4 to 8.9 years; 54 males) was scanned while they
 294 watched Inscapes, a movie paradigm designed for collecting resting-state data to reduce potential head motion. In addition,
 295 a subject-level covariate was included in the analysis: the overall theory of mind ability based on a parent-report measure
 296 (the theory of mind inventory, or ToMI). fMRI images were acquired with the following EPI scan parameters: $B_0 = 3$ T,
 297 flip angle = 70° , echo time = 25 ms, repetition time = 2000 ms, 36 slices, planar field of view = 192×192 mm², voxel size
 298 = $3.0 \times 3.0 \times 3.5$ mm³, 210 volumes with a total scanning time of 426 seconds. Twenty-one ROIs (Table 3) were selected
 299 from the literature because of their potential relevancy to the current study, and they were neither chosen nor defined per
 300 the whole brain analysis results of the current data. Mean Fisher-transformed z-scores were extracted at each ROI from
 301 the output of seed-based correlation analysis (seed: right temporo-parietal junction at the MNI coordinates of (50, -60,
 302 18)) from each of the 124 subjects. The effect of interest at the population level is the relationship at each brain region
 303 between the behavioral measure of the overall ToMI and the region’s association with the seed. A whole brain analysis
 304 showed the difficulty of some clusters surviving FWE correction (Table 2).

305 The data from the 21 ROIs were analyzed through the modeling triplets, GLMs (14) and (15), LME (16) and BML
 306 (17), with the effect of interest at the j th ROI being the relationship between ToMI and the ROI’s association with the
 307 seed: $\theta_{1j} = b_1 + \xi_{1j}$. The exchangeability assumption for LME and BML was deemed reasonable because, prior to the
 308 analysis, no specific information was available regarding the order and relatedness of the effects across subjects and ROIs.
 309 It is worth noting that the data were skewed with a longer right tail than left (black solid curve in Fig. 3a and Fig. 3b).
 310 When fitted at each ROI separately with GLM (simple regression in this case) using the overall ToMI as an explanatory
 311 variable, the model yielded lackluster fitting (Fig. 3a) in terms of skewness, the two tails, and the peak area. As shown in
 312 Fig. 1, five ROIs (R PCC, R TPJp, L IPL, L TPJ, and L aMTS/aMTG) reached a two-tailed significance level of 0.05,
 313 and two ROIs (PCC/PrC and vmPFC) achieved a two-tailed significance level of 0.1 (or one-tailed significance level of
 314 0.05 if directionality was *a priori* known). However, the burden of FWE correction (e.g., Bonferroni) for the ROI-based
 315 approach with univariate GLM is so severe that none of the ROIs could survive the penalizing metric.

Table 2: ROIs and FWE correction for their associated clusters^a

voxel-wise p	cluster threshold	number of surviving ROIs	ROIs
0.001	28	2	R PCC, PCC/PrC
0.005	66	4	R PCC, PCC/PrC., L IPL, L TPJ
0.01	106	4	R PCC, PCC/PrC., L IPL, L TPJ
0.05	467	4	R PCC, PCC/PrC., L IPL, L TPJ
0.05*	467	(4)	(L aMTS/aMTG, R TPJp, vmPFC, dmPFC)

^aMonte Carlo simulations were conducted using a mixed exponential spatial autocorrelation function (Cox et al., 2017) instead of FWHM to determine the cluster threshold (voxel size: $3 \times 3 \times 3 \text{ mm}^3$). The ROI abbreviations are listed in Table 3.

*Special note for the last row (voxel-wise p -value of 0.05): four ROIs including L IPL, L TPJ, R PCC, PCC/PrC survived together with their clusters from the FWE correction, and the other four ROIs listed here (L aMTS/aMTG, R TPJp, vmPFC, and dmPFC) did not survive with their clusters but showed some evidence of effect when the cluster size requirement was dropped.

Table 3: MNI coordinates of the 21 ROIs^a

No	ROI	Coordinates (x, y, z)
1	R PCC	(8, -59, 35)
2	R TPJp	(56, -56, 25)
3	R Insula	(49, -8, -11)
4	L IPL	(-55, -65, 27)
5	L SFG	(-7, 58, 21)
6	R IFG (BA45)	(47, 22, 6)
7	R IFG (BA9)	(60, 25, 19)
8	L MTG	(-51, -62, 5)
9	L CG	(-5, 8, 42)
10	L IFG	(-46, 24, 7)
11	ACC	(0, 38, 10)
12	SGC	(-2, 32, -8)
13	PCC/PrC	(-2, -52, 26)
14	dmPFC	(-2, 5, 14)
15	L TPJ	(-46, -66, 18)
16	L vBG	(-6, 10, -8)
17	R vBG	(6, 10, -8)
18	L aMTS/aMTG	(-54, -10, -20)
19	R Amy/Hippo	(24, -8, -22)
20	L Amy/Hippo	(-24, -10, -20)
21	vmPFC	(-2, 50, -10)

^aThe 21 ROIs were chosen because of their potential involvement for the current experiment based on previous studies. Each ROI was created as a ball with a center at the coordinates (in millimeters) from the literature (Xiao et al., 2017) and a radius of 6 mm. ROI abbreviations: L, left hemisphere; R, right hemisphere; PCC/PrC, precuneus/posterior cingulate cortex; TPJp, posterior temporo-parietal junction; IPL, inferior parietal lobe; SFG, superior frontal gyrus; IFG, inferior frontal gyrus; aMTS/aMTG, anterior middle temporal sulcus/gyrus; CG, cingulate gyrus; ACC, anterior cingulate cortex; SGC, subgenual cingulate cortex; dmPFC, dorsomedial prefrontal cortex; vBG, ventral basal ganglia; Amy/Hippo, amygdala/hippocampus; vmPFC, ventromedial prefrontal cortex.

(a) Comparisons: LME and BML

Term	LME		BML				
	Estimate	SD	Estimate	SD	95% QI	ESS	\hat{R}
$sd(\xi_0)$	0.153	-	0.162	0.027	[0.118, 0.225]	551	1.00
$sd(\xi_1)$	0.008	-	0.009	0.002	[0.005, 0.014]	947	1.00
$corr(\xi_0, \xi_1)$	0.88	-	0.773	0.161	[0.366, 0.985]	1054	1.00
$sd(\pi)$	0.076	-	0.077	0.006	[0.066, 0.091]	500	1.01
b_0	0.168	0.034	0.167	0.036	[0.094, 0.241]	162	1.03
b_1	0.007	0.004	0.007	0.004	[-0.001, 0.015]	468	1.00
σ	0.153	-	0.153	0.002	[0.149, 0.157]	2000	1.00

(b) Comparisons: GLM and BML

Model	LOOIC	SE
GLM	-300.39	98.25
BML	-2247.06	86.42
GLM - BML	1946.67	96.35

Table 4: Comparisons among GLM, LME and BML. (a) The seed-based correlation results at 21 ROIs from 124 subjects were fitted with LME (using the R package lme4) and BML (using Stan with 4 chains and 1,000 iterations) separately, in which overall ToMI was an explanatory variable. Random effects under LME correspond to group/entity-level effects plus family specific parameters (standard deviation σ for the residuals ϵ_{ij}) under BML, while fixed effects under LME correspond to population-level effects under BML. The column headers SD, QI, and ESS are short for standard deviation, quantile interval, effect sample size, respectively. The parameter estimates from the LME and BML outputs (columns in gray) are very similar, even though priors were injected into BML. All \hat{R} values under BML were less than 1.1, indicating that all the 4 chains converged well. The effective sizes for the population- and group/entity-level effect of ToMI were 468 and 947, respectively, enough to warrant quantile accuracy in summarizing the posterior distributions. Comparisons between GLM and BML. (b) To directly compare with BML, the Bayesianized version of GLM (15) was fitted with the data, and the higher predictive accuracy of BML is seen here with its substantial lower out-of-sample deviance measured by the leave-one-out information criterion (LOOIC), the widely applicable (or Watanabe-Akaike) information criterion (WAIC) through leave-one-out cross-validation, and the corresponding standard error (SE).

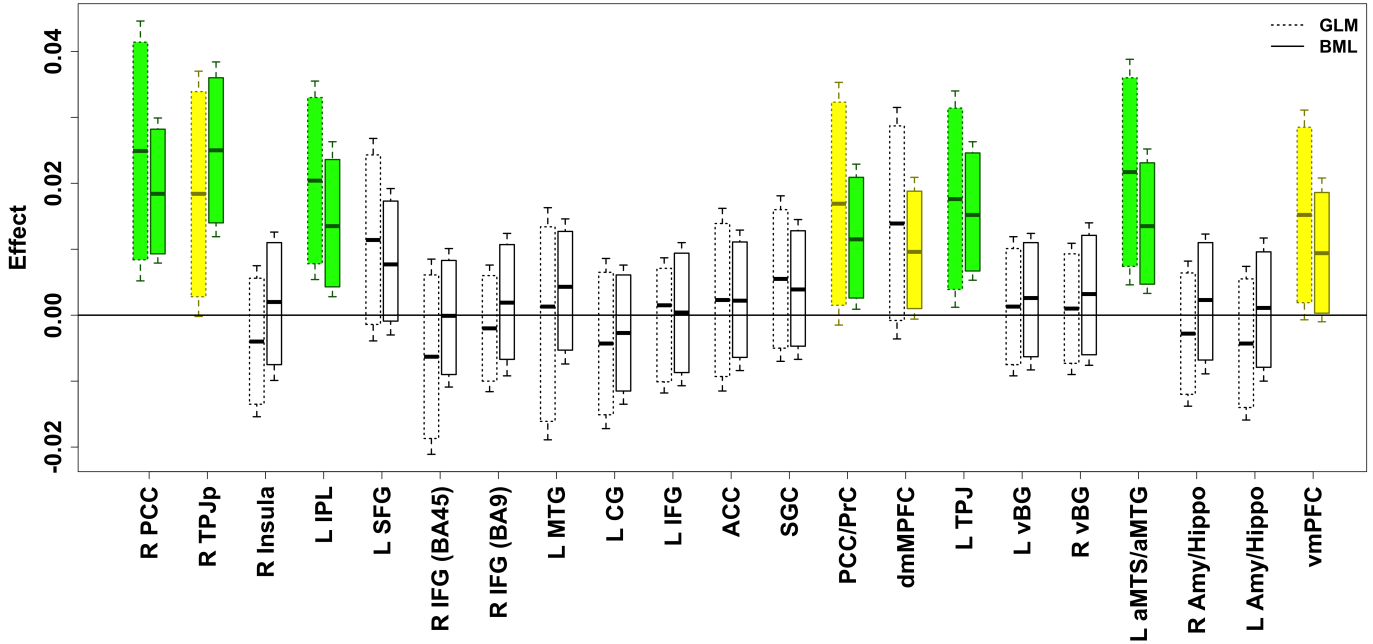
316 The ROI data were fitted with LME (16) and BML (17) using the overall ToMI as an explanatory variable through,
317 respectively, the R (R Core Team, 2017) package lme4 (Bates et al., 2015) and Stan with the code translated to C++
318 and compiled. Runtime for BML was 5 minutes including approximately 1 minute of code compilation on a Linux system
319 (Fedora 25) with AMD Opteron 6376 at 1.4 GHz. All the parameter estimates at the population level were quite similar
320 between the two models (Table 4(a)), indicating that the weakly informative priors we adopt for hyperparameters in BML
321 had little impact on parameter estimation. However, of interest here are the effects at the entity (i.e., ROI), not population,
322 level, which could be derived through BML but not LME. As for those effects at the ROI level, compared to the traditional
323 ROI-based GLM, the shrinkage under BML can be seen in Fig. 1: most effect estimates were dragged toward the center.
324 Similar to the ROI-based GLM without correction, BML demonstrated (Figures 1 and 2) strong evidence within 95%
325 quantile interval of the overall ToMI effect at six ROIs (R PCC, R TPJp, L IPL, PCC/PrC, L TPJ, and L aMTS/aMTG),
326 and within 90% (or 95% if directionality was *a priori* known) quantile interval at two additional ROIs (dmMPFC and
327 vmPFC).

328 One exception to the general shrinkage under BML is that the median effect, 0.025, at the region of R TPJp (second
329 row in the table and box plot of Fig. 1) was actually higher than that under GLM, 0.018. Such an exception occurred
330 because the final result is a combination or a tug of war between the shrinkage impact as shown in (8) and the correlation
331 structure among the ROIs as shown in (9). Noticeably, the quality and fitness of BML can be diagnosed and verified
332 through posterior predictor check (Fig. 3a and Fig. 3b) that compares the observed data with the simulated data based
333 on the model: not only did BML accommodate the skewness of the data better than GLM, but also did the partial pooling
334 render much better fit for the peak and both tails as well. Cross validation through LOO (Table 4(b), Fig. 3c and Fig. 3d)
335 also manifested the advantage of BML fitting over GLM. Nevertheless, there is still room for the improvement of BML:
336 the peak area could be fitted better, which may require nonlinearity or incorporating other potential covariates.

337 One apparent aspect that the ROI-based BML excels is the completeness and transparency in results reporting: if
338 the number of ROIs is not overwhelming (e.g., less than 100), the summarized results for every ROI can be completely
339 presented in a tabular form (*c.f.* Fig. 1) and in full distributions of posterior density (Fig. 2). It is worth emphasizing that
340 Bayesian inferences focus less on the point estimate of an effect and its associated quantile interval, but more on the whole
341 posterior density as shown in Fig. 2 that offers more detailed information about the effect uncertainty. Unlike the whole
342 brain analysis in which the results are typically reported as the tips of icebergs above the water, posterior density reveals
343 the spread, shape and skewness regardless of the statistical evidence. In addition, one does not have to stick to a single
344 harsh thresholding when deciding a criterion on the ROIs for discussion; for instance, even if an ROI lies outside of, but
345 close to, the 95% quantile interval (e.g., dmMPFC and vmPFC in Figures 1 and 2), it can still be reported and discussed as

ROI \ result	ToMI effect		standard error		2.5%		5%		95%		97.5%	
	GLM	BML	GLM	BML	GLM	BML	GLM	BML	GLM	BML	GLM	BML
R PCC	0.025	0.018	0.010	0.006	0.005	0.008	0.008	0.009	0.041	0.028	0.045	0.030
R TPJp	0.018	0.025	0.009	0.007	-0.000	0.012	0.003	0.014	0.034	0.036	0.037	0.038
R Insula	-0.004	0.002	0.006	0.006	-0.015	-0.010	-0.014	-0.008	0.006	0.011	0.007	0.013
L IPL	0.020	0.014	0.008	0.006	0.005	0.003	0.008	0.004	0.033	0.024	0.035	0.026
L SFG	0.011	0.008	0.008	0.006	-0.004	-0.003	-0.001	-0.001	0.024	0.017	0.027	0.019
R IFG (BA45)	-0.006	0.000	0.007	0.005	-0.021	-0.011	-0.019	-0.009	0.006	0.008	0.008	0.010
R IFG (BA9)	-0.002	0.002	0.005	0.005	-0.012	-0.009	-0.010	-0.007	0.006	0.011	0.008	0.012
L MTG	-0.001	0.004	0.009	0.005	-0.019	-0.007	-0.016	-0.005	0.013	0.013	0.016	0.015
L CG	-0.004	-0.003	0.007	0.005	-0.017	-0.014	-0.015	-0.011	0.007	0.006	0.009	0.008
L IFG	-0.002	0.000	0.005	0.005	-0.012	-0.011	-0.010	-0.009	0.007	0.009	0.009	0.011
ACC	0.002	0.002	0.007	0.005	-0.012	-0.008	-0.009	-0.006	0.014	0.011	0.016	0.013
SGC	0.006	0.004	0.006	0.005	-0.007	-0.007	-0.005	-0.005	0.016	0.013	0.018	0.014
PCC/PrC	0.017	0.012	0.009	0.005	-0.001	0.001	0.002	0.003	0.032	0.021	0.035	0.023
dmMPFC	0.014	0.010	0.009	0.005	-0.004	-0.001	-0.001	0.001	0.029	0.019	0.032	0.021
L TPJ	0.018	0.015	0.008	0.005	0.001	0.005	0.004	0.007	0.031	0.025	0.034	0.026
L vBG	0.001	0.003	0.005	0.005	-0.009	-0.008	-0.007	-0.006	0.010	0.011	0.012	0.012
R vBG	0.001	0.003	0.005	0.005	-0.009	-0.008	-0.007	-0.006	0.009	0.012	0.011	0.014
L aMTS/aMTG	0.022	0.013	0.009	0.006	0.005	0.003	0.007	0.005	0.036	0.023	0.039	0.025
R Amy/Hippo	-0.003	0.002	0.006	0.005	-0.014	-0.009	-0.012	-0.007	0.006	0.011	0.008	0.012
L Amy/Hippo	-0.004	0.001	0.006	0.005	-0.016	-0.010	-0.014	-0.008	0.005	0.010	0.007	0.012
vmPFC	0.015	0.009	0.008	0.006	-0.001	-0.001	0.002	0.000	0.029	0.019	0.031	0.021

The table columns with the label GLM are the results from 21 separate GLMs (14); however, the GLM (15) with pooled variance and flat priors rendered very similar inferences (not shown). The percentages show the percentile confidence intervals for the conventional GLM with no pooling and the quantile intervals for BML, respectively. Rows in green indicate that the corresponding effect lies beyond the positive domain of the 95% quantile interval under BML, revealing strong evidence for the behavior effect; rows in yellow indicate that the corresponding effect lies beyond the positive domain of the 90% quantile interval under BML (or the 95% quantile interval if the effect sign is *a priori* known), revealing moderate evidence for the behavior effect. The conventional ROI-based GLM revealed a similar pattern but with different effect estimates and distributions due to the isolated treatment among the ROIs; however, none of the 21 ROIs would survive FWE correction under NHST. Unlike the popular practice of sharp thresholding under NHST, more customized quantile intervals (e.g., 10%, 50% and 90%), if desirable, can be added in the final reporting in order to make corresponding inferences.



The same results in the table are shown in box plots. The ToMI effect is plotted with the horizontal black bar in the middle of each box as the mean for GLM or median for BML; each box (or whisker pair) represents the 90% (or 95%) confidence interval for GLM (dashed) or quantile interval for BML (solid). Among all ROIs except R TPJp, the shrinkage or pooling effect of BML is evident in the sense that the effects are dragged from the extremes to the center.

Figure 1: Comparisons of results between the conventional GLM and BML

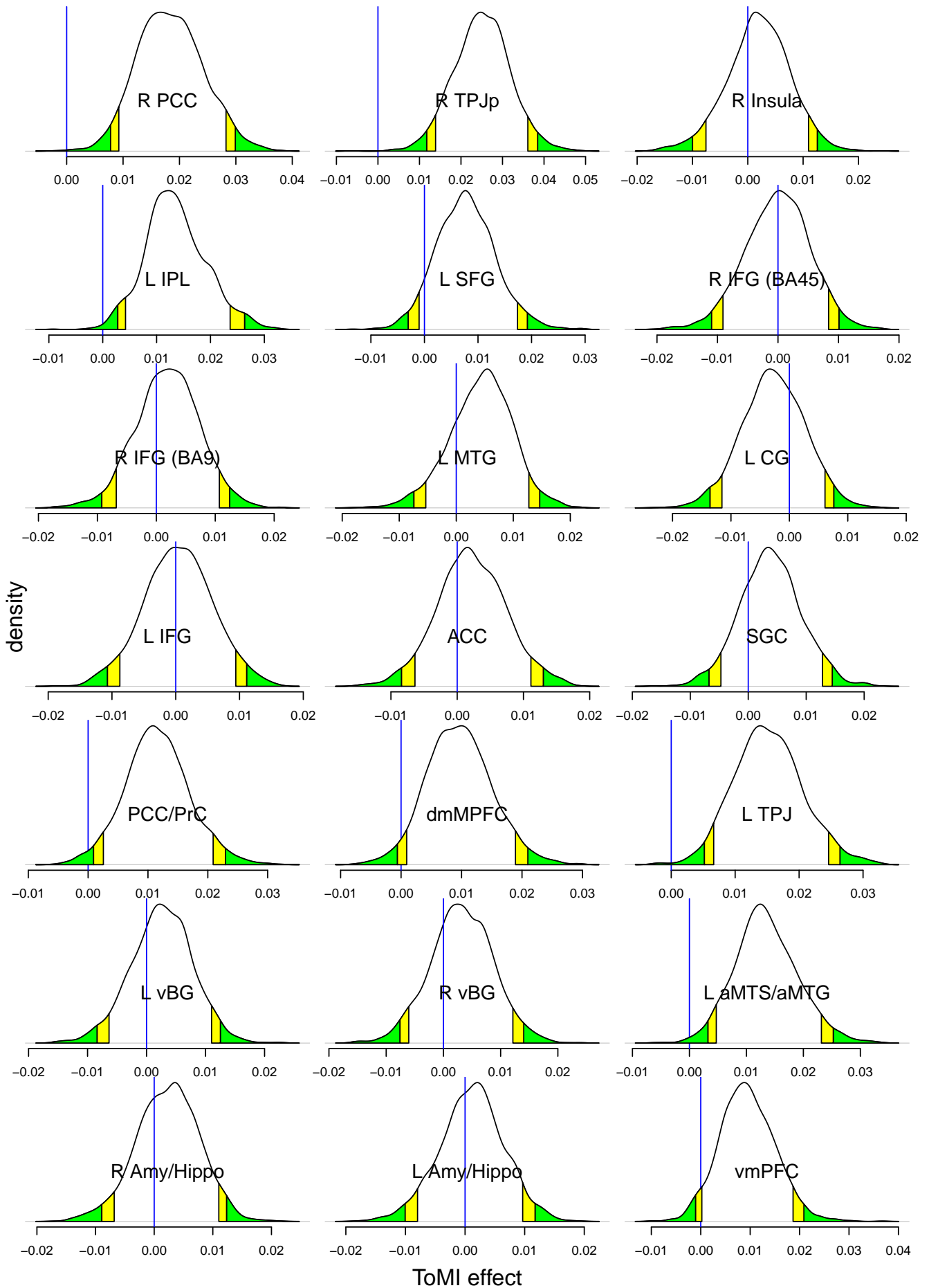


Figure 2: Posterior density distributions based on 2000 draws from BML. The vertical blue line indicates zero ToMI effect, yellow and green tails mark the 90% and 95% quantile intervals, respectively, and the ROIs with strong evidence of ToMI effect can be identified as the blue line being within the color tails. Compared to the conventional confidence interval that is flat and inconvenient to interpret, the posterior density provides much richer information about each effect such as spread, shape and skewness.

346 long as all the details are revealed. Such flexibility and transparency are difficult to navigate or maneuver through cluster
347 thresholding at the whole brain level. As a counterpart to NHST, a probability metric could still be provided for each
348 effect under BML in the sense as illustrated in Table 5; however, we opt not to do so for two reasons: 1) such a probability
349 measure could be easily misinterpreted in the NHST sense, and, more importantly, 2) it is the predictive intervals shown
350 in Fig. 1 and the complete posterior distributions illustrated in Fig. 2, not the single probabilities, that fully characterize
351 the posterior distribution, providing richer information than just binary (“in or out”) thresholding.

352 Interestingly, those four regions (L IPL, L TPJ, R PCC, PCC/PrC) that passed the FWE correction at the voxel-
353 wise p -cutoff of 0.005 (Table 2) in the whole brain analysis were confirmed with the ROI-based BML (Figures 1 and 2).
354 Moreover, another four regions (L aMTS/aMTG, R TPJp, vmPFC, dmPFC) revealed some evidence of ToMI effect under
355 BML. In contrast, these four regions did not stand out in the whole brain analysis after the application of FWE correction
356 at the cluster level regardless of the voxel-wise p -threshold (Table 2), even though they would have been evident if the
357 cluster size requirement were not as strictly imposed.

358 Discussion

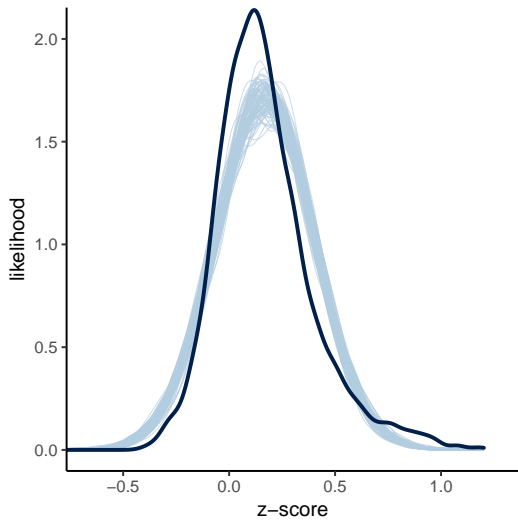
359 Applied to the neuroimaging context, BML adopts partial pooling and can be considered as a trade-off between two
360 extreme modeling choices (Appendix D): complete pooling and no pooling. Complete pooling assumes no variations among
361 the entities (voxels, regions, or surface nodes); that is, all entities are assumed to be identical or homogeneous. Because
362 of the omnipresence of regional heterogeneity in the brain, nobody would be interested in such a modeling strategy in
363 neuroimaging, but it serves here as an extreme anchor for the convenience of comparison. In contrast, no pooling, currently
364 adopted in massively univariate modeling, fully trusts the data, and offers the best fit separately for each individual entity
365 to the current data at hand. As a consequence, each entity is considered autonomous and independent with each other in
366 the analytical model. To some extent, the current approaches pool the information across the neighboring voxels in the step
367 of controlling FPR through clusterization. However, there are two huge disadvantages associated with no pooling: it carries
368 the risk of overfitting, poor inference or prediction for future data; and, to control for multiplicity and overconfidence, the
369 current approaches compromise in efficiency by paying the price in over-penalizing small regions through leveraging the
370 spatial extent.

371 Through an adaptively regularizing prior (e.g., Gaussian distribution among brain regions), partial pooling achieves a
372 counterbalance between homogenization and autonomy. Specifically, BML treats each entity as a substantiation generated
373 through a random process that adaptively regularizes the entities, and it conservatively pools the effect of each entity
374 toward the center. In other words, the methodology sacrifices model performance in the form of a poorer fit in samples
375 (observed data) for the sake of better interfere and better fit (prediction) out of samples (future data) through partial
376 pooling (McElreath, 2016). Therefore, BML may fit each region individually worse than univariate GLM, but BML excels
377 in collective fitting and overall model performance. It is this counterbalance through regularization that effectively controls
378 the errors of incorrect sign and incorrect magnitude; and as a byproduct, BML leverages the multiplicity issue and equally
379 treats all regions purely based on their signal strength, regardless of their spatial size.

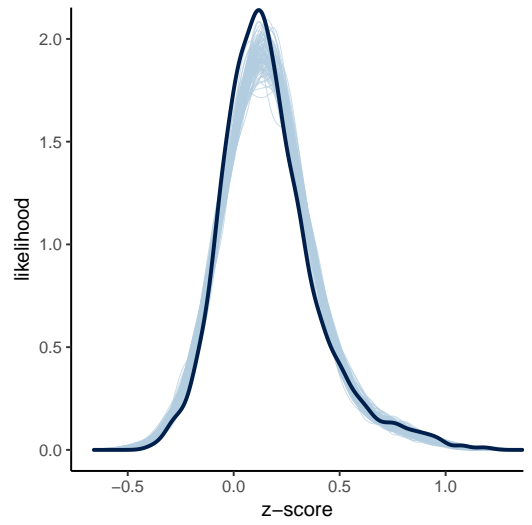
380 Current approaches to correcting for FPR

381 Arbitrariness is involved in the multiple testing correction of parametric methods. In the conventional statistics frame-
382 work, the thresholding bar ideally plays the role of winnowing the wheat (true effect⁶) from the chaff (random noise), and
383 a p -value of 0.05 is commonly adopted as a benchmark for comfort in most fields. However, one big problem facing the
384 correction methods for multiple testing is the arbitrariness surrounding the thresholding, in addition to the arbitrariness of
385 0.05 itself. Both Monte Carlo simulations and random field theory start with a voxel-wise probability threshold (e.g., 0.01,
386 0.005, 0.001) at the voxel (or node) level, and a spatial threshold is determined in cluster size so that overall FPR can be
387 properly controlled at the cluster level. If clusters are analogized as islands, each of them may be visible at a different sea
388 level (voxel-wise p -value). As the cluster size based on statistical filtering plays a leveraging role, with a higher statistical
389 threshold leading to a smaller cluster cutoff, a neurologically or anatomically small region can only gain ground with a low
390 p -value while large regions with a relatively large p -value may fail to survive the criterion. Similarly, a lower statistical
391 threshold (higher p) requires a higher cluster volume, so smaller regions have little chance of reaching the survival level.

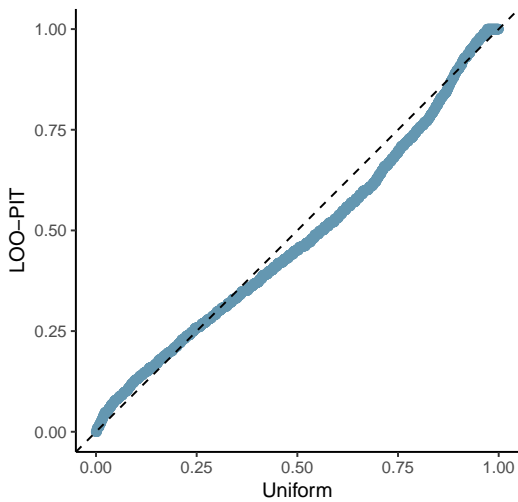
⁶Needless to say, the concept of *true* effect only makes sense under the current model framework at hand, and may not hold once the model is revised.



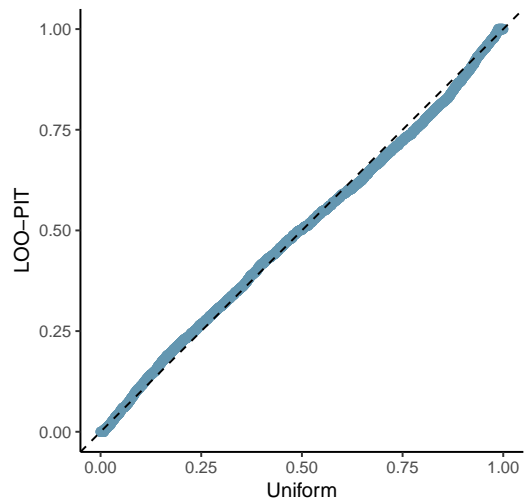
(a) GLM posterior predictive density



(b) BML posterior predictive density



(c) GLM cross-validation: Q-Q plot (uniform)



(d) BML cross-validation: Q-Q plot (uniform)

Figure 3: Model performance comparisons through posterior predictive checks and cross validations between conventional univariate GLM (*a* and *c*) and BML (*b* and *d*). The subfigures *a* and *b* show the posterior predictive density overlaid with the raw data from the 124 subjects at the 21 ROIs for GLM and BML, respectively: solid black curve is the raw data at the 21 ROIs with linear interpolation while the fat curve in light blue is composed of 100 sub-curves each of which corresponds to one draw from the posterior distribution based on the respective model. The differences between the two curves indicate how well the respective model fits the raw data. BML fitted the data better than GLM at the peak and both tails as well as the skewness because pooling the data from both ends toward the center through shrinkage clearly validates our adoption of BML. The subfigures *c* and *d* contrast GLM and BML through cross-validation with leave-one-out log predictive densities through the calibration of marginal predictions from 100 draws; the calibration is assessed by comparing probability integral transformation (PIT) checks to the standard uniform distribution. The diagonal dashed line indicates a perfect calibration: there are some suboptimal calibration for both models, but BML is clearly a substantial improvement over GLM. To simulate the posterior predictive data for the conventional ROI-based approach (*a* and *c*), the Bayesianized version of GLM (15) was adopted with a noninformative uniform prior for the population parameters.

392 In addition, this arbitrariness in statistical threshold at the voxel level poses another challenge for the investigator: one
393 may lose spatial specificity with a low statistical threshold since small regions that are contiguous may get swamped by
394 the overlapping large spatial extent; on the other hand, sensitivity may have to be compromised for large regions with
395 low statistic values when a high statistical threshold is chosen. A recent critique on the rigor of cluster formation through
396 parametric modeling (Eklund et al., 2016) has resulted in a trend to require a higher statistical thresholding bar (e.g., with
397 the voxel-wise threshold below 0.005 or even 0.001); however, the arbitrariness persists because this trend only shifts the
398 probability threshold range.

399 Permutation testing is limited in modeling capability. For example, it shares the same limitations as univariate GLM
400 in handling missing data and sophisticated random-effects structures; in addition, it does not have an effective approach to
401 taking into consideration the reliability of effect estimates. Furthermore, it has its share of arbitrariness in multiple testing
402 correction too. As an alternative to parametric methods, an early version of permutation testing (Nichols and Holmes,
403 2001) bears similar arbitrary issues. It starts with the construction of a null distribution through permutations in regard to
404 a maximum statistic (either maximum testing statistic or maximum cluster size based on a predetermined threshold for the
405 testing statistic). The original data are assessed against the null distribution, and the top winners at a designated rate (e.g.,
406 5%) among the testing statistic values or clusters will be declared as the surviving ones. While the approach is effective in
407 maintaining the nominal FWE level, two problems are embedded with the strategy. First of all, the spatial properties are
408 not directly taken into consideration in the case of maximum testing statistic. For example, an extreme case to demonstrate
409 the spatial extent issue is that a small cluster (or even a single voxel) might survive the permutation testing as long as its
410 statistic value is high enough (e.g., $t(20) = 6.0$) while a large cluster with a relatively small maximum statistic value (e.g.,
411 $t(20) = 2.5$) would fail to pass the filtering. The second issue is the arbitrariness involved in the primary thresholding
412 for the case of maximum cluster size: a different primary threshold may end up with a different set of clusters. That is,
413 the reported results may likely depend strongly on an arbitrary threshold. Addressing these two problems, a later version
414 of permutation testing (Smith and Nichols, 2009) takes an integrative consideration between signal strength and spatial
415 relatedness, and thus solves both problems involving the earlier version of permutation testing⁷. Such an approach has
416 been implemented in programs such as Randomise and PALM in FSL using threshold-free cluster enhancement (TFCE)
417 (Smith and Nichols, 2009) and in 3dttest++ in AFNI using equitable thresholding and clusterization (ETAC) (Cox, 2018).
418 Nevertheless, the adoption of permutations in neuroimaging, regardless of the specific version, is not directly about the
419 concern of distribution violation as in the classical nonparametric setting (in fact, a pseudo- t value is still computed at
420 each voxel in the process); rather, it is the randomization among subjects in permutations that creates a null distribution
421 against which the original data can be tested at the whole brain level.

422 We argue that spatial size as a correction leverage unnecessarily pays the cost of lower identification power to achieve
423 the nominal false positive level. All of the current correction methods, parametric and nonparametric, are still meant to
424 use spatial extent or the combination of spatial extent and signal strength as a filter to control the overall FPR at the whole
425 brain level. They all share the same hallmark of sharp thresholding at a preset acceptance level (e.g., 5%) under NHST, and
426 they all use spatial extent as a leverage, penalizing regions that are anatomically small and rewarding large smooth regions
427 (Cremers et al., 2017). The combination of signal strength and spatial extent adopted in the recent permutation methods
428 such as TFCE and ETAC are advantageous in addressing the issue of arbitrariness of primary thresholding in the cluster-
429 based correction methods and the primary permutation approach. Nevertheless, such a method of “extent and height” still
430 discriminates spatially small regions, even though slightly less so. For instance, between two brain regions with the same
431 signal strength, the anatomically larger one would be easier to pass the current approaches including TFCE and ETAC
432 than its smaller counterpart; between one case with one isolated region and another with two or more contiguous regions,
433 the former may fail to pass the current filtering methods even with a stronger signal strength. Due to the unforgiving
434 penalty of correction for multiple testing, some workaround solutions have been adopted by focusing the correction on a
435 reduced domain instead of the whole brain. For example, the investigator may limit the correction domain to gray matter
436 or regions based on previous studies. Putting the justification for these practices aside, accuracy is a challenge in defining
437 such masks; in addition, spatial specificity remains a problem, shared by the typical whole brain analysis, although to a
438 lesser extent.

⁷A single voxel is still possible, but much less likely, to survive this correction approach.

Questionable practices of correction for FPR under NHST

Univariate GLM is inefficient in handling neuroimaging data. It may work reasonably well if the following two conditions can be met: 1) no multiple testing, and 2) high signal-to-noise ratio (strong effect and high precision measurement) as illustrated in the lower triangular part of the table or right side of the curves in Fig. 4 (Appendix B). However, neither of the two conditions is likely satisfied with typical neuroimaging data. Due to the stringent requirements of correction for multiple testing across thousands of resolution elements in neuroimaging, a daunting challenge facing the community is the power inefficiency or high type II errors under NHST. Even if prior information is available as to which ROIs are potentially involved in a study, an ROI-based univariate GLM would still be obliged to share the burden of correction for multiplicity equally and agnostically to any such knowledge. The modeling approach usually does not have the luxury to survive the penalty, as shown with our experimental data in the table of Fig. 1, unless only a few ROIs are included in the analysis. Furthermore, with many low-hanging fruits with relatively strong signal strength (e.g., 0.5% signal change or above) having been largely plucked, the typical effect under investigation nowadays is usually subtle and likely small (e.g., in the neighborhood of 0.1% signal change). Compounded with the presence of substantial amount of noise and suboptimal modeling (e.g., ignoring the HDR shape subtleties), detection power is usually low. It might be counterintuitive, but one should realize that the noisier or more variable the data, the less one should be confident about any inferences based on statistical significance, as illustrated with the type S and type M errors in Figure 5 (Appendix B). With fixed threshold correction approaches, small regions are hard to funnel through the FPR criterion even if their effect magnitude is the same as or even higher than those larger regions. Even for approaches that take into consideration both spatial extent and effect magnitude (TFCE, ETAC), small regions remain disadvantaged when their effect magnitude is at the same level as their larger counterparts.

Furthermore, dichotomous thinking and decision-making under NHST are usually not fully compatible with the underlying mechanism under investigation. Current knowledge regarding brain activations has not reached a point where one can make accurate dichotomous claims as to whether a specific brain region under a condition is activated or not; lack of underlying “ground truth” has made it difficult to validate any but the most basic models. The same issue can be raised about the binary decision as to whether the response difference under two conditions is either the same or different. Therefore, a pragmatic mission is to detect activated regions in terms of practical, instead of statistical, significance. The conventional NHST runs against the idealistically null point H_0 , and declares a region having no effect based on statistical significance with a safeguard set for type I error. When the power is low, not only reproducibility will suffer, but also the chance of having an incorrect sign for a statistically significant effect be substantial (Fig. 4 and Fig. 5). Only when the power reaches 30% or above does the type S error rate become low. Publication bias due to the thresholding funnel contributes to type S and type M errors as well. The sharp thresholding imposed by the widely adopted NHST strategy uses a single threshold through which a high-dimension dataset is funneled. An ongoing debate has been simmering for a few decades regarding the legitimacy of NHST, ranging from cautionary warning against misuses of NHST (Wasserstein and Lazar, 2016), to tightening the significance level from 0.05 to 0.005 (Benjamin et al., 2017), to totally abandoning NHST as a gatekeeper (McShare et al., 2017; Amrhein and Greenland, 2017). The poor controllability of type S and type M errors is tied up with widespread problems across many fields. It is not a common practice nor a requirement in neuroimaging to report the effect estimates; therefore, power analysis for a brain region under a task or condition is largely obscure and unavailable, let alone the assessment of type S and type M errors.

Lastly, reproducibility may deteriorate through inefficient modeling and dichotomous inferences. Relating the discussion to the neuroimaging context, the overall or global FPR is the probability of having data as extreme as or more extreme than the current result, under the assumption that the result was produced by some “random number generator,” which is built into algorithms such as Monte Carlo simulations, random field theory, and randomly shuffled data as pseudo-noise in permutations. It boils down to the question: are the data truly pure noise (even though spatially correlated to some extent) in most brain regions? Since controlling for FPR hinges on the null hypothesis of no effect, p -value itself is a random variable that is a nonlinear continuous function of the data at hand, therefore it has a sampling distribution (e.g., uniform(0,1) distribution if the null model is true). In other words, it might be under-appreciated that even identical experiments would not necessarily replicate an effect that is dichotomized in the first one as statistically significant (Lazzeroni et al., 2016). The common practice of reporting only the statistically significant brain regions and comparing to those nonsignificant regions based on the imprimatur of statistic- or p -threshold can be misleading: the difference between a highly significant region and a nonsignificant region could simply be explained by pure chance. The binary emphasis on statistical significance unavoidably leads to an investigator only focusing on the significant regions and diverting attention

away from the nonsignificant ones. More importantly, the traditional whole brain analysis usually leads to selectively report surviving clusters conditional on statistical significance through dichotomous thresholding, potentially inducing type M errors, biasing estimates with exaggerated effect magnitude, as illustrated in Fig. 5. Rigor, stringency, and reproducibility are lifelines of science. We think that there is more room to improve the current practice of NHST and to avoid information waste and inefficiency. Because of low power in fMRI studies and the questionable practice of binarized decisions under NHST, a Bayesian approach combined with integrative modeling offers a platform to more accurately account for the data structure and to leverage the information across multiple levels.

What Bayesian modeling offers

Bayesian inferences are usually more compatible with the research, not null, hypothesis. Almost all statistics consumers (including the authors of this paper) were *a priori* trained within the conventional NHST paradigm, and their mindsets are usually familiar with and entrenched within the concept and narratives of *p*-value, type I error, and dichotomous interpretations of results. Out of the past shadows cast by the theoretical and computation hurdles, as well as the image of subjectivity, Bayesian methods have gradually emerged into the light. One direct benefit of Bayesian inference, compared to NHST, is its concise, intuitive and straightforward interpretation, as illustrated in Table 5. For instance, among its controversies (Morey et al., 2016), the conventional confidence interval weighs equally all possible values a parameter could take within the interval, regardless of how implausible some of them are; in contrast, the quantile interval under Bayesian framework is more subtly expressed through the corresponding posterior density (Fig. 2). Even though the NHST modeling strategy literally falsifies the straw man H_0 , the real intention is to confirm the alternative (or research) hypothesis through rejecting H_0 ; in other words, the falsification of H_0 is only considered an intermediate step under NHST, and the ultimate goal is the confirmation of the intended hypothesis. In contrast, under the Bayesian paradigm, the investigator’s hypothesis is directly placed under scrutiny through incorporating prior information, model checking and revision. Therefore, the Bayesian paradigm is more fundamentally aligned with the hypothetico-deductivism axis along the classic view of falsifiability or refutability by Karl Popper (Gelman and Shalizi, 2013).

Table 5: Interpretation differences between NHST and Bayesian framework

	Probability p	Effect Interval $[L, U]$
NHST	If H_0 is true, the probability of having the current result or more extreme is p (based on what would have occurred under other possible datasets); e.g., $P(T(\mathbf{y}) > t_c \text{easy} = \text{difficult}) = p$, where $T(\mathbf{y})$ is a statistic (e.g., Student’s t) based on data \mathbf{y} and t_c is a threshold.	If the study is exactly repeated an infinite number of times, the percentage of those confidence intervals will cover the true effect is $1 - p$; e.g., $P(L \leq \text{easy} - \text{difficult} \leq U) = 1 - p$, where “easy - difficult” is treated as being fixed while L and U are random.
Bayesian	The probability of having the <i>current</i> result being different from zero is p (given the dataset); e.g., $P(\text{easy} - \text{difficult} < L \text{ or } \text{easy} - \text{difficult} > U \mathbf{y}) = p$, where L and U are lower and upper bounds of the $(1 - p)100\%$ quantile interval.	The probability that the effect falls in the predictive interval is $1 - p$ (given the data); e.g., $P(L \leq \text{easy} - \text{difficult} \leq U \mathbf{y}) = 1 - p$, where “easy - difficult” is considered random while L and U are known conditional on data \mathbf{y} .

In addition to interpretational convenience, Bayesian modeling is less vulnerable to the amount of data available and to the issue of multiple testing. Conventional statistics heavily relies on large sample size and asymptotic property; in contrast, Bayesian inferences bear a direct interpretation conditional on the data regardless of sample size. Practically speaking, should we fully “trust” the effect estimate at each ROI or voxel at its face value? Some may argue that the effect estimate from the typical neuroimaging individual or population analysis has the desirable property of unbiasedness, as asymptotically promised by central limit theory. However, in reality the asymptotic behavior requires a very large sample size, a luxury difficult for most neuroimaging studies to reach. As the determination of a reasonable sample size depends on signal strength, brain region, and noise level, the typical sample size in neuroimaging tends to get overstretched, creating a hotbed for a low power situation and potentially high type S and type M errors. Another fundamental issue with the conventional univariate modeling approach in neuroimaging is the two-step process: first, pretend that the voxels or nodes are independent with each other, and build a separate model for each spatial element; then, handle the multiple testing issue using spatial relatedness to only partially, not fully, recoup the efficiency loss. In addition to the conceptual novelty for those with little experience outside the NHST paradigm, BML simplifies the traditional two-step workflow with one integrative model, fully shunning the multiple testing issue.

527 Through integrative incorporation across ROIs, the BML approach renders conservative effect estimation in place of
528 controlling FPR. Unlike the p -value under NHST, which represents the probability of obtaining the current data generated
529 by an imaginary machinery (e.g., assuming that no effect exists), a posterior distribution for an effect under the Bayesian
530 framework directly and explicitly shows the uncertainty of our current knowledge conditional on the current data and the
531 prior model. From the Bayesian perspective, we should not put too much faith in point estimates. In fact, not only should
532 we not fully trust the point estimates from GLM with no pooling, but also should we not rely too much on the centrality
533 (median, mean) of the posterior distribution from a Bayesian model. Instead, the focus needs to be placed more on the
534 uncertainty, which can be visualized through the posterior distributions or characterized by the quantile intervals of the
535 posterior distribution if summarization is required. Specifically, BML, as demonstrated here with the ROI data, is often
536 more conservative in the sense that it does not “trust” the original effect estimates as much as GLM, as shown in Fig. 1;
537 additionally, in doing so, it fits the data more accurately than the ROI-based GLM (Table 4(b) and Fig. 3). Furthermore,
538 the original multiple testing issue under the massively univariate platform is deflected within one unified model: it is the
539 type S, not type I, errors that are considered crucial and controlled under BML. Even though the posterior inferences at
540 the 95% quantile interval in our experimental data were similar to the statistically significant results at the 0.05 level under
541 NHST, BML in general is more statistically conservative than univariate GLM under NHST, as shown with the examples
542 in Gelman et al. (2012).

543 We reiterate that the major difference is the assumption about the brain regions: noninformative flat prior for the
544 conventional GLM versus the Gaussian assumption for BML. With a uniform prior, all values on the real axis are equally
545 likely; therefore, no information is shared across regions under GLM. On the other hand, it is worth mentioning that the
546 Gaussian assumption for the priors including the likelihood under a Bayesian model is based on two considerations: one
547 aspect is convention and pragmatism, and the other aspect is the fact that, per maximum entropy principle, the most
548 conservative distribution is Gaussian if the data have a finite variance (McElreath, 2016). However, a Bayesian model
549 tends to be less sensitive to the model (likelihood or prior for the data in Bayesian terminology); in other words, even
550 though the true data-generating process is always unknown, a model is only a convenient framework or prior knowledge
551 to start with the Bayesian updating process so that a Bayesian model is usually less vulnerable to assumption violations.
552 In contrast, statistical inferences with conventional approaches heavily rely on the sampling distribution assumptions.
553 Through adaptive regularization, BML achieves a goal to trade off poorer fit in sample for better inference and improved
554 fit out of sample (McElreath, 2016); the amount of regularization is learned from the data through partial pooling that
555 embodies the similarity assumption of effects among the brain regions. From the NHST perspective, BML can still commit
556 type I errors, and its FPR could be higher under some circumstances than, for example, its GLM counterpart. Such type I
557 errors may sound alarmingly serious; however, the situation is not as severe as its appearance for two reasons: 1) the concept
558 of FPR and the associated model under NHST are framed with a null hypothesis, which is not considered pragmatically
559 meaningful in the Bayesian perspective; and 2) in reality, inferences under BML most likely have the same directionality as
560 the true effect because type S errors are well controlled across the board under BML (Gelman and Teulinckx, 2000). Just
561 consider which of the following two scenarios is worse: (a) when power is low, the likelihood under the NHST to mistakenly
562 infer that the BOLD response to easy condition is higher than difficult could be sizable (e.g., 30%), and (b) with the type
563 S error rate controlled below, for example, 3.0%, the BML might exaggerate the magnitude difference between difficult and
564 easy conditions by, for example, 2 times. While not celebrating the scenario (b), we expect that most researchers would
565 view the scenario (a) as more problematic.

566 Prior assignment is an intrinsic component of Bayesian modeling. [As the priors are non-informative for the parameters
567 of the BML models considered here at the population level, there is no extra information injected.](#) Therefore, one somewhat
568 controversial aspect of Bayesian modeling is the adoption of a prior for each hyperparameter at the entity level, and that the
569 prior is meshed with the data and gets updated into the posterior distribution. Some may consider that an Achilles’ heel of
570 Bayesian modeling is its subjectivity with respect to prior selection at the entity level. First of all, we would argue that, to
571 start with, every model, Bayesian or non-Bayesian, is a prior or likelihood function in the sense that the analyst presumes
572 a distribution for the data (e.g., Gaussian distribution in the conventional GLMs (1), (2), and (3)). Secondly, weakly
573 informative priors are even routinely adopted by conventional statistics in approaches such as penalized likelihood in ridge
574 regression and LASSO. Priors are chosen, evaluated and revised just as any components and assumptions in the model.
575 The inherent subjectivity of BML is no more than are model assumptions (e.g. Gaussian distribution) for conventional
576 statistics as well as different opinions of analytical approaches, different outliers handling methods and processing steps
577 in neuroimaging. Furthermore, priors are applied at the epistemological, not ontological level (McElreath, 2016); with no
578 intention to get tangled in the epistemological roots or the philosophical debates of subjectivity versus objectivity, we simply

579 divert the issue to the following suggestion (Gelman and Hennig, 2017): replacing the term “subjectivity” with “multiple
580 perspectives and context dependence,” and, in lieu of “objectivity,” focusing on transparency, consensus, impartiality, and
581 correspondence to observable reality. Therefore, our focus here is the pragmatic aspect of Bayesian modeling: with prior
582 distributions, we can make inferences for each ROI under BML, which cannot be achieved under LME.

583 Prior selection in Bayesian modeling is usually well justified. Since noninformative priors are adopted for population
584 effects here, the only impact of prior information incorporated into BML comes from two aspects: the distributional
585 assumptions about those entities such as subjects and ROIs, and the hyperpriors. However, the rationale for the Gaussian
586 priors of entities is not more far-fetched than that for the Gaussian assumption of cross-subject distribution in the typical
587 GLM adopted in neuroimaging group analysis. As for the hyperpriors, weakly informative priors basically play the role of
588 numerical regularization: when the amount of data is moderate or large, these conservative priors levy a negligible effect on
589 the final inferences; on the other hand, when the data do not contain enough information for robust inferences, the weakly
590 informative priors prevent the distributions from becoming unsupportively dispersive. Specifically, for simple models such
591 as Student’s t -test and GLM, Bayesian approach renders similar inferences if noninformative priors are assumed. On the
592 surface a noninformative prior does not “artificially” inject much “subjective” information into the model, and should be
593 preferred. In other words, it might be considered a desirable property from the NHST viewpoint, since noninformative
594 priors are independent of the data. Because of this “objectivity” property, one may insist that noninformative priors should
595 be used all the time. Counterintuitively, a noninformative prior may become so informative that it could cause unbounded
596 damage (Gelman et al., 2017). If we analyze the r ROIs individually as in the r GLMs (14), the point estimate for each
597 effect θ_j is considered stationary, and we would have to correct for multiple testing due to the fact that r separate models are
598 fitted independently. Bonferroni correction would likely be too harsh, which is the major reason that ROI-based analysis is
599 rarely adopted in neuroimaging except for effect verification or graphic visualization. On the other hand, the conventional
600 approach with the r GLMs (14) is equivalent to the BML (17) by *a priori* assuming an improper flat prior for θ_j with the
601 cross-ROI variability $\tau^2 = \infty$; that is, each effect θ_j can be any value with equal likelihood within $(-\infty, \infty)$. In the case
602 of BOLD response, it is not necessarily considered objective to adopt a noninformative prior such as uniform distribution
603 when intentionally ignoring the prior knowledge. In fact, we do have the prior knowledge that the typical effect from a
604 3T scanner has the same scale and lies within, for example, $(-4, 4)$ in percent signal change; this commonality can be
605 utilized to calibrate or regularize the noise, extreme values, or outliers due to pure chance or unaccounted-for confounding
606 effects (Gelman et al., 2012), which is the rationale for our prior Gaussian assumption for both subjects and ROIs. A
607 flat noninformative prior or no investigator choice does not necessarily mean objectivity. Even for an effect for a covariate
608 (e.g., the associate between behavior and BOLD response), it would be far-fetched to assume that τ^2 has the equal chance
609 between, for example, 0 and 10^{10} . Another example of information waste under NHST is the following. Negative or zero
610 variance can occur in an ANOVA model while zero variance may show up in LME. Such occurrences are usually due to
611 the full reliance on the data or a parameter boundary, and such direct estimates are barely meaningful: an estimate of
612 cross-subject variability $\lambda^2 = 0$ in (17) indicates that all subjects have absolutely identical effects. However, a Bayesian
613 inference is a tug of war between data and priors, and therefore negative or zero variance inferences would not occur because
614 those scenarios from the data are regularized by the priors, as previously shown in ICC computations that are regularized
615 by a Gamma prior for the variance components (Chen et al., 2017c).

616 In typical neuroimaging data with reasonable number of subjects and moderate number of ROIs, the weakly informative
617 priors for scaling parameters usually play a nudging role. In general, when there is enough data, weakly informative priors
618 are usually drowned out by the information from the data; on the other hand, when data are meager (e.g., with small or
619 moderate sample size), such priors can play the role of regularization (Gelman et al., 2017) so that smoother and more
620 stable inferences could be achieved than would be obtained with a flat prior. In addition, a weakly informative prior for
621 BML allows us to make reasonable inferences at the region level while model quality can be examined through tools such
622 as posterior predictive check and LOO cross-validation. Therefore, if we do not want to waste such prior knowledge for an
623 effect bounded within a range in the brain, the commonality shared by all the brain regions can be incorporated into the
624 model through a weakly informative prior and the calibration of partial pooling among the ROIs, thus eliding the step of
625 correcting for multiple testing under NHST.

626 To summarize, we recommend that three types of priors be adopted for ROI-based BML: 1) Gaussian distribution for
627 the response variable (or input data) and effects at the entity level such as ROIs and subjects, 2) uninformative prior
628 for the effects (e.g., intercept and slopes) at the population level, and 3) weakly informative priors for scaling parameters
629 (e.g., variances). Such a prior setting should be able to handle the typical BML modeling in neuroimaging unless the
630 amount of data is overly meager (e.g., a few ROIs or subjects only). With the typical neuroimaging dataset, our prior

631 recommendation would have negligible impact on the population effect estimates as shown in the comparisons between
632 LME and BML (Table 4(a)). However, it is worth noting that the effects of interest here are not those at the population
633 level under the LME and BML framework, but rather those effects at the entity (i.e. ROI) level in the current context.
634 We note that the experiment dataset employed here to demonstrate BML applications happens to have more than 100
635 subjects. However, such a large sample size is not a prerequisite for BML. A larger sample would lead to more robust
636 inferences (as it would in other approaches); however, BML does not require more subjects than the rule of thumb with
637 typical neuroimaging group model such as GLM in terms of sample size.

638 Progress in Bayesian computations is paving the way for more advanced modeling opportunities. Bayesian algorithms
639 have traditionally been burdened with meticulous and time consuming computations, making their adoption for wide
640 applications difficult and impractical for multilevel models even with a dataset of small or moderate size. However, the
641 situation has been substantially ameliorated by the availability of multiple software tools such as Stan, and the rapid
642 development in Stan over the past few years has promoted the wide adoption of Bayesian modeling. In particular, Stan
643 adopts static HMC Samplers and its extension, NUTS, and it renders less autocorrelated and more effective draws for the
644 posterior distributions, achieving quicker convergence than the traditional Bayesian algorithms such as Metropolis-Hastings,
645 Gibbs sampling, and so on. With faster convergence and high efficiency, it is now feasible to perform full Bayesian inferences
646 for BML with datasets of moderate size.

647 Advantages of ROI-based BML

648 Bayesian modeling has long been adopted in neuroimaging at the voxel or node level (e.g., Woolrich et al., 2004; Penny
649 et al., 2005; Westfall et al., 2017; Eklund et al., 2017; Mejia et al., 2017); nevertheless, correction for FWE would still
650 have to be imposed as part of the model or as an extra step. In the current context, we formulate the data generation
651 mechanism for each dataset through a progressive triplet of models on a set of ROIs: $GLM \rightarrow LME \rightarrow BML$. The strength
652 of multilevel modeling lies in its capability of stratifying the data in a hierarchical or multilevel structure so that complex
653 dependency or correlation structures can be properly accounted for coherently within a single model. Specifically applicable
654 in neuroimaging is a crossed or factorial layout between the list of ROIs and subjects as shown in the LME equation (4)
655 and its Bayesian counterpart (5). Our adoption of BML, as illustrated with the demonstrative data analysis, indicates that
656 BML holds some promise for neuroimaging and offers the following advantages over traditional approaches:

657 1) As BML and LME usually share a corresponding modeling structure, BML can handle data structures involved in
658 the conventional models that are subsumed under LME such as Student’s t -tests, ANOVA, regression, ANCOVA and GLM.
659 For example, missing data can be handled as long as the missingness can be considered missing at random. Furthermore,
660 BML is superior to LME in dealing with complicated data structures. For example, the number of parameters under
661 LME with a sophisticated variance-covariance structure could be high, leading to overfitting and convergence failure with the
662 maximum likelihood algorithm; in contrast, the numerical regularization under BML may help overcome the overfitting
663 and convergence issues.

664 2) Compared to the conventional GLM, BML achieves a better model performance and higher predictive accuracy
665 through partial pooling, a trade-off between underfitting with complete pooling and overfitting with no pooling. Specifically,
666 BML is assessed with data through adaptive regularization with nudges from the prior information: it learns from the data
667 and borrows information across ROIs to improve the quality of individual estimates and posterior distributions with the
668 assumption of similarity among the regions.

669 3) Instead of separately correcting for multiple testing, BML incorporates multiple testing as part of the model by
670 assigning a prior distribution among the ROIs (i.e., treating ROIs as random effects under the LME paradigm). In doing
671 so, multiple testing is handled under the scaffold of the multilevel data structure by conservatively shrinking the original
672 effect toward the center; that is, instead of leveraging cluster size or signal strength, BML leverages the commonality among
673 ROIs.

674 4) BML may achieve higher spatial specificity through efficient modeling. A statistically identified cluster through a
675 whole brain analysis is not necessarily anatomically or functionally meaningful. In other words, a statistically identified
676 cluster is not always aligned well with a brain region for diverse reasons such as “bleeding” effect due to contiguity among
677 regions, and suboptimal alignment to the template space, as well as spatial blurring. In fact, such a cluster may overlap
678 multiple brain regions or subregions; for example, with a large sample size (e.g., more 200 subjects), one may have
679 difficulty in differentiating statistically identified regions within a large portion of the brain that all pass even a very
680 stringent threshold (e.g., voxel-wise significance level of 10^{-10}). In contrast, as long as a region can be *a priori* defined, its

681 statistical inference under BML is assessed by its signal strength relative to its peers, not by its spatial extent, providing
682 an alternative to the whole brain analysis with more accurate spatial specificity.

683 5) BML offers a flexible approach to dealing with double sidedness at the ROI level. When prior information about
684 the directionality of an effect is available on some, but not all, regions (e.g., from previous studies in the literature), one
685 may face the issue of performing two one-tailed t -tests at the same time in a blindfold fashion due to the limitation of the
686 massively univariate approach. The ROI-based approach disentangles the complexity since the posterior inference for each
687 ROI can be made separately.

688 6) Model validation is a crucial facet of Bayesian framework. It is sometimes stated a model- or assumption-free
689 approach is preferable to parametric methods, for example, with the argument that the p -value from permutation testing
690 can be considered “exact.” However, it should be noted that “exactness” in this sense is a technical definition, requiring
691 strict exchangeability and based on the assumption that the only possible values obtainable in an experiment were obtained.
692 That is, the p -value’s “exactness” remains conditional on the current data. This emphasis on strict exactness under the
693 NHST is questionable since the p -value itself is a random variable and the data are usually quite noisy; for instance, a
694 repeated experiment under the same conditions would lead to a different “exact” p -value. Furthermore, uncertainty or
695 precision information is usually not provided for the clusters identified from permutation testing (as well as other cluster-
696 based approaches), and no model checking capability is offered either even though a linear model is indeed defined under
697 the typical framework (including permutation testing) in neuroimaging.

698 On the other hand, just as the Ptolemaic model served as a starting point for the supersession with the Heliocentric
699 model of Copernicus, Galileo and Kepler, so does a parametric framework, regardless of its limitations, set up a scaffold that
700 allows more modeling capabilities and targeted inferences. Those capabilities and inferences can be validated, criticized
701 and incrementally improved. It may be trite to cite the famous quote of “all models are wrong” by George E. P. Box.
702 However, the reality in neuroimaging is that model quality checks have historically been substantially lacking. When
703 prompted, one may acknowledge the potential problems and pitfalls of a model, but it is much more common to see
704 statistical analyses conducted as mechanical operations on assembly lines; when discussing and reporting results from the
705 model, the investigator tends to treat the model as if it were always true and then discusses statistical inferences without
706 realizing the implications or ramifications of a model that fits poorly or even conflicts with data. Building, comparing,
707 tuning and improving models is a daunting task with whole brain data due to the high computational cost and visualization
708 inconvenience. In contrast, model quality checking is an intrinsic part of Bayesian modeling process, such as providing
709 quantile intervals for each effect estimate. The performance of each model and the room for improvement can be directly
710 examined through graphical display as shown in Fig. 3.

711 7) A full results reporting is possible for all ROIs under BML. The conventional NHST focuses on the point estimate of
712 an effect supported with statistical evidence in the form of a p -value. In the same vein, typically the results from the whole
713 brain analysis are displayed with sharp-thresholded maps or tables that only show the surviving clusters with statistic- or
714 p -values. In contrast, as the focus under the Bayesian framework is on the predictive distribution, not the point estimate,
715 of an effect, the totality of BML results can be summarized in a table as shown in Figures 1 and 2, listing the predictive
716 intervals in various quantiles (e.g., 50%, 75%, and 95%), a luxury that whole brain analysis cannot provide. Such totality
717 pits against the backdrop in which the effect estimates and their uncertainty are usually not reported in the whole brain
718 analysis (Chen et al., 2017b). In contrast, BML modeling at the ROI level directly allows the investigator to present
719 the effect estimate. More importantly, BML substantiates the reporting advantage not only because of modeling at the
720 ROI level, but also due to the fact that the uncertainty associated with each effect estimate can demonstrated in a much
721 richer fashion (e.g., explicit revealing the spread or skewness of the posterior distribution) through the posterior density
722 distribution (Fig. 2) than the conventional confidence interval (1) that is flat and inconvenient to interpret. Furthermore,
723 the full results reporting from BML would substantially improve future meta analysis, unlike the current meta analysis that
724 is largely based on the anatomical coordinates of one voxel without taking into consideration the effect size information
725 across studies.

726 8) To some extent, the ROI-based BML approach can alleviate the arbitrariness involved in the thresholding with the
727 current FPR correction practices. Even though BML allows the investigator to present the whole results for all regions,
728 for example, in a table format, we do recognize that the investigator may prefer to focus the discussion on some regions
729 with strong posterior evidence. In general, with all effects reported in totality, regardless of their statistical evidence, the
730 decision of choosing which effects to discuss in a paper should be based on cost, benefit, and probabilities of all results
731 (Gelman et al., 2014). Specifically for neuroimaging data analysis, the decision still does not have to be solely from the
732 posterior distribution; instead, we suggest that the decision be hinged on the statistical evidence from the current data,

733 combined with prior information from previous studies. For example, one may still choose the 95% quantile interval as an
734 equivalent benchmark to the conventional p -value of 0.05 when reporting the BML results. However, those effects with,
735 say, 90% quantile intervals excluding 0 can still be discussed with a careful and transparent description, which can be used
736 as a reference for future studies to validate or refute; or, such effects can be reported if they have been shown in previous
737 studies. Moreover, rather than a cherry-picking approach on reporting and discussing statistically significant clusters in
738 whole brain analysis⁸ showing neither the effect magnitude nor the corresponding uncertainty, we recommend a principled
739 approach in results reporting in which the ROI-based results be reported in totality with a summary as shown in Figures
740 1 and 2 and be discussed through transparency and soft, instead of sharp, thresholding. We believe that such a soft
741 thresholding strategy is more healthy and wastes less information for a study that goes through a strenuous pipeline of
742 experimental design, data collection, and analysis.

743 Limitations of ROI-based BML and future directions

744 ROIs can be specified through several ways depending on the specific study or information available regarding the
745 relevant regions. For example, one can find potential regions involved in a task or condition including resting state from
746 the literature. Such regions are typically reported as the coordinates of a “peak” voxel (usually highest statistic value
747 within a cluster), from which each region could be defined by centering a ball with a radius of, e.g., 6 mm in the brain
748 volume (or by projecting an area on the surface). Regions can also be located through (typically coordinate-based) meta
749 analysis with databases such as NeuroSynth (<http://www.neurosynth.org>) and BrainMap (<http://www.brainmap.org>),
750 with tools such as `brain_matrix` (https://github.com/fredcallaway/brain_matrix), GingerALE (<http://brainmap.org/ale>),
751 Sleuth (<http://brainmap.org/sleuth>), and Scribe (<http://www.brainmap.org/scribe>) that are associated with the database
752 BrainMap. Anatomical atlases (e.g., <http://surfer.nmr.mgh.harvard.edu>, <http://www.med.harvard.edu/aanlib>) and func-
753 tional parcellations (e.g., Schaefer et al., 2017) are another source of region definition. As a different strategy, by recruiting
754 enough subjects, one could use half of the subjects to define ROIs, and the other half to perform ROI-based analysis;
755 similarly, one could scan the same set of subjects longer, use the first portion of the data to define ROIs, and the rest to
756 perform ROI-based analysis.

757 One concern is that the exchangeability requirement of BML assumes that no differential information is available across
758 the ROIs in the model. Exchangeability captures symmetry among the ROIs in a sense that does not require independence.
759 That is, an independent and identically distributed set of ROIs is exchangeable, but not vice versa. However, every
760 exchangeable set of ROIs is identically distributed. Under some circumstances, ROIs can be expected to share some
761 information and not fully independent, especially when they are anatomically contiguous or more functionally related than
762 the other ROIs (e.g., homologous regions in opposite hemisphere). However, the exchangeability is an epistemological,
763 neither physical nor ontological, assumption that renders a convenient approximation of a prior distribution by a mixture
764 of i.i.d. distributions (de Finetti’s theorem). The presence of temporal correlation in time series regression may cause the
765 underestimation of variances because the conventional statistics heavily relies on the concept of degrees of freedom. In
766 contrast, Bayesian inferences build on posterior distributions without invoking the degrees of freedom, and the violation of
767 exchangeability usually leads to negligible effect on the final shape of posterior distributions except for the precise sequence
768 in which the posterior draws occur (McElreath, 2016). Furthermore, the performance of BML can be effectively examined
769 through posterior predictive checks and cross validations, as illustrated in Fig. 3. **Further improvement may be possible
770 through future modeling work on exploring the possibility of capturing the finer structures among the ROIs.**

771 It might be tempting to apply the BML strategy to the whole brain voxel-wise analysis (e.g., shrinking the effects
772 among voxels). However, such an extension faces serious issues, such as daunting computational cost and the loss of spatial
773 specificity. Nevertheless, BML with ROIs defined from a whole brain atlas could be a viable solution. Other limitations of
774 the ROI-based BML are as follows.

775 1) Just as the FWE correction on the massively univariate modeling results is sensitive to the size of the full domain
776 in which it is levied (whole brain, gray matter, or a user-defined volume), so the results from BML will depend to some
777 extent on the number of ROIs (or which) ones included. For a specific ROI j , changing the composition among the
778 rest of ROIs (e.g., adding an extra ROI or replacing one ROI with another) may result in a different prior distribution
779 (e.g., $\theta_j \sim N(\mu, \tau^2)$ in BML (5)) and a different posterior distribution for θ_j . However, it merits noting that the regions
780 should not be arbitrarily chosen but rather selected from the current knowledge and relevancy of the involving effect under
781 investigation.

⁸A popular cluster reporting method among the neuroimaging software packages is to simply present the investigator only with the icebergs above the water, the surviving clusters, reinforcing the illusionary either-or dichotomy under NHST.

2) ROI data extraction involves averaging among voxels within the region. Averaging, as a spatial smoothing or low-pass filtering process, condenses, reduces or dilutes the information among the voxels (e.g., 30) within the region to one number, and loses any finer spatial structure within the ROI. In addition, the variability of extracted values across subjects and across ROIs could be different from the variability at the voxel level.

3) ROI-based analysis is conditional on the availability and quality of the ROI definition. One challenge facing ROI definition is the inconsistency in the literature due to inaccuracies across different coordinate/template systems and publication bias. In addition, some extent of arbitrariness is embedded in ROI definition; for example, a uniform adoption of a fixed radius may not work well due to the heterogeneity of brain region sizes. When not all regions or subregions currently can be accurately defined, or when no prior information is available to choose a region in the first place, the ROI-based approach may miss any potential regions if they are not included in the model.

Despite these limitations, we believe that BML holds its unique promising potentials and advantages over the conventional approaches, and we hope that it will serve as a catalyst for a wider modeling landscape in neuroimaging. As shown here, the performance of BML can be directly assessed and compared to the conventional approaches through posterior predictive checks and cross validations. Admittedly, as all models are idealized statistical representations, our BML work presented here is only an incremental step in neuroimaging; besides multiplicity, NHST pitfalls and inefficient modeling, there remain daunting challenges such as linearity assumption (e.g., superposition among overlapping hemodynamic responses), temporal correlation (Olszowy et al., 2017) and the inaccuracy of presumed hemodynamic response modeling in FMRI data analysis.

Conclusion

The prevalent adoption of dichotomous decision making under NHST runs against the continuous nature of most quantities under investigation, including neurological responses, which has been demonstrated to be problematic through type S and type M errors when the signal-to-noise ratio is low. The conventional correction for FWE in neuroimaging data analysis is viewed as a “desirable” standard procedure for whole brain analysis because the criterion is a pivotal component of NHST. However, it is physiologically unfeasible to claim that there is absolutely no effect in most brain regions; therefore, we argue that setting the stage only to fight the straw man of no effect anywhere is not necessarily a powerful nor efficient inference strategy. Inference power is further compromised by FWE correction due to the inefficiency involved in the massively univariate modeling approach. As BOLD responses in the brain share the same scale and range, the ROI-based BML approach proposed here allows the investigator to borrow strength and effectively regularize the distribution among the regions. Furthermore, no unnecessary penalization is levied on small regions under BML simply because of their anatomical structure, thus BML can simultaneously achieve meaningful spatial specificity and detection efficiency. Lastly, BML can provide increasing transparency on model building, quality control, and detailed results reporting, and offers a promising approach to addressing two multiplicity issues: multiple testing and double sidedness.

Information Sharing Statement

We have implemented the BML methodology into a program, `BayesianGroupAna.py`, that is available as part of the publicly distributed AFNI suite at <https://afni.nimh.nih.gov>. In addition, the experiment dataset and the executable script can be downloaded at the AFNI website <https://tinyurl.com/yb2tzbqq>

Acknowledgments

The research and writing of the paper were supported (GC, PAT, and RWC) by the NIMH and NINDS Intramural Research Programs (ZICMH002888) of the NIH/HHS, USA, and by the NIH grant R01HD079518A to TR and ER. Much of the modeling work here was inspired from Andrew Gelman’s blog. We are indebted to Paul-Christian Bürkner and the Stan development team members Ben Goodrich, Daniel Simpson, Jonah Sol Gabry, Bob Carpenter, and Michael Betancourt for their help and technical support. The simulations were performed in the R language for statistical computing and the figures were generated with the R package `ggplot2` (Wickham, 2009).

Appendix A. Pitfalls of NHST

- i. It is a common mistake by investigators and even statistical analysts to misinterpret the conditional probability under NHST as the posterior probability of the truth of the null hypothesis (or the probability of the null event conditional on the current data at hand) even though fundamentally $P(data | H_0) \neq P(H_0 | data)$.
- ii. One may conflate statistical significance with practical significance, and subsequently treat the failure to reach statistical significance as the nonexistence of any meaningful effect. Even though the absence of evidence is not an evidence of absence, it is common to read discussions in scientific literature wherein the authors implicitly (or even explicitly) treat statistically non-significant effects as if they were zero.
- iii. Statistic- or p -values cannot easily be compared: the difference between a statistically significant effect and another effect that fails to pass the significance level does not necessarily itself reach statistical significance.
- iv. How should the investigator handle the demarcation, due to sharp thresholding, between one effect with $p = 0.05$ (or a surviving cluster cutoff of 54 voxels) and another with $p = 0.051$ (or a cluster size of 53 voxels)⁹?
- v. The focus on statistic- or p -value seems to, in practice, lead to the preponderance of reporting only statistical, instead of effect, maps in neuroimaging, losing an effective safeguard that could have filtered out potentially spurious results (Chen et al., 2017b).
- vi. One may mistakenly gain more confidence in a statistically significant result (e.g., high statistic value) in the context of data with relatively heavy noise or with a small sample size (e.g., leading to statement such as “despite the small sample size” or “despite the limited statistical power”). In fact, using statistical significance as a screener can lead researchers to make a wrong assessment about the sign of an effect or drastically overestimate the magnitude of an effect.
- vii. While the conceptual classifications of false positives and false negatives make sense in a system of discrete nature (e.g., juror decision on H_0 : the suspect is innocent), what are the consequences when we adopt a mechanical dichotomous approach to assessing a quantity of continuous, instead of discrete, nature?
- viii. It is usually under-appreciated that the p -value, as a function of data, is a random variable, and thus itself has a sampling distribution. In other words, p -values from experiments with identical designs can differ substantially, and statistically significant results may not necessarily be replicated (Lazzeroni et al., 2016).

Appendix B. Type S and type M errors

We discuss two types of error that are not often discussed in neuroimaging: type S and type M. These two types of error cannot be directly captured by the FPR concept and may become severe when the effect is small relative to the noise, which is usually the situation in BOLD neuroimaging data. In the NHST formulation, we formulate a null hypothesis H_0 (e.g., the effect of an easy task E is identical to a difficult one D), and then commit a type I (or false positive) error if wrongly rejecting H_0 (e.g., the effect of easy is judged to be statistically significantly different from difficult when actually their effects are the same); in contrast, we make a type II (or false negative) error when accepting H_0 when H_0 is in fact false (e.g., the effect of easy is assessed to be not statistically significant from difficult even though their effects do differ). These are the dichotomous errors associated with NHST, and the counterbalance between these two types of error are the underpinnings of typical experimental design as well results reporting.

However, we could think about other ways of framing errors when making a statistical assessment (e.g., the easy case elicits a stronger BOLD response at some region than the difficult case) conditional on the current data. We are exposed to a risk that our decision is contrary to the truth (e.g., the BOLD response to the easy condition is actually lower than to the difficult condition). Such a risk is gauged as a type S (for “sign”) error when we incorrectly identify the sign of the effect; its values range from 0 (no chance of error) to 1 (full chance of error). Similarly, we make a type M (for “magnitude”) error when estimating the effect as small in magnitude if it is actually large, or when claiming that the effect is large in magnitude if it is in fact small (e.g., saying that the easy condition produces a *much* large response than the difficult one when actually the difference is tiny); its values range across the positive real numbers: [0, 1) correspond to underestimation

⁹The investigator would not be able to even see such borderline clusters since the typical software implementations mechanically adopt a dichotomous results presentation.

869 of effect magnitude, 1 describes correct estimation, and $(1, \infty^+)$ mean overestimation. The two error types are illustrated
870 in Fig. 5 for inferences made under NHST. In the neuroimaging realm, effect magnitude is certainly a property of interest,
871 therefore the corresponding type S and type M errors would be of research interest.

872 Geometrically speaking, if the null hypothesis H_0 can be conceptualized as the point at zero, NHST aims at the real
873 space \mathbf{R} excluding zero with a pivot at the point of zero (e.g., $D - E = 0$); in contrast, type S error gauges the relative
874 chance that a result is assessed on the wrong side of the distribution between the two half spaces of \mathbf{R} (e.g., $D - E > 0$
875 or $D - E < 0$), and type M error gauges the relative magnitude of differences along segments of \mathbf{R}^+ (e.g., the ratio of
876 *measured* to *actual* effect is $\gg 1$ or $\ll 1$). Thus, we characterize type I and type II errors as “point-wise” errors, driven
877 by judging the equality, and describe type S and type M errors as “direction-wise,” driven by the focus of inequality or
878 directionality.

879 One direct application of type M error is that publication bias can lead to type M errors, as large effect estimates are
880 more likely to filter through the dichotomous decisions in statistical inference and reviewing process. Using the type S and
881 type M error concepts, it might be surprising for those who encounter these two error types for the first time to realize
882 that, when the data are highly variable or noisy, or when the sample size is small with a relatively low power (e.g., 0.06), a
883 statistically significant result at the 0.05 level is quite likely to have an incorrect sign – with a type S error rate of 24% or
884 even higher (Gelman and Carlin, 2014). In addition, such a statistically significant result would have a type M error with
885 its effect estimate much larger (e.g., 9 times higher) than the true value. Put it another way, if the real effect is small and
886 sampling variance is large, then a dataset that reaches statistical significance must have an exaggerated effect estimate and
887 the sign of the effect estimate is likely to be incorrect. Due to the ramifications of type M errors and publication filtering,
888 an effect size from the literature could be exaggerated to some extent, seriously calling into question the usefulness of
889 power analysis under NHST in determining sample size or power, which might explain the dramatic contrast between the
890 common practice of power analysis as a requirement for grant applications and the reproducibility crisis across various
891 fields. Fundamentally, power analysis inherits the same problem with NHST: a narrow emphasis on statistical significance
892 is placed as a primary focus (Gelman and Carlin, 2013).

893 The typical effect magnitude in BOLD fMRI at 3 Tesla is usually small, less than 1% signal change in most brain
894 regions except for areas such as motor and primary sensory cortex. Such a weak signal can be largely submerged by the
895 overwhelming noise and distortion embedded in the fMRI data. The low power for detection of typical fMRI data analyses
896 in typical datasets is further compounded by the modeling challenges in accurately capturing the effect. For example, even
897 though large number of physiological confounding effects are embedded in the data, it is still difficult to properly incorporate
898 the physiological “noises” (cardiac and respiratory effects) in the model. Moreover, habituation, saturation, or attenuation
899 across trials or within each block are usually not considered, and such fluctuations relative to the average effect would be
900 treated as noise or fixed- instead of random-effects (Westfall et al., 2017). There are also strong indications that a large
901 portion of BOLD activations are usually unidentified at the individual subject level due to the lack of power (Gonzalez-
902 Castillo et al., 2012). Because of these factors, the variance due to poor modeling overwhelms all other sources (e.g., across
903 trials, runs, and sessions) in the total data variance (Gonzalez-Castillo et al., 2016); that is, the majority (e.g., 60-80%) of
904 the total variance in the data is not properly accounted for in statistical models.

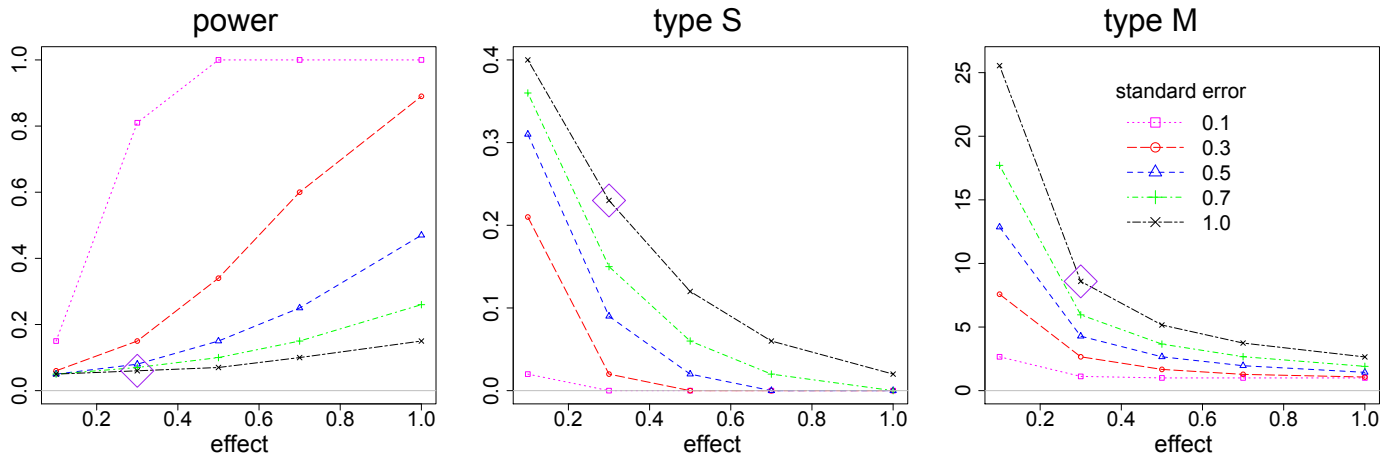
905 Appendix C. Multiplicity in neuroimaging

906 In general, we can classify four types of multiplicity issues that commonly occur in neuroimaging data analysis.

907 A) *Multiple testing.* The first and major multiplicity arises when the same design (or model) matrix is applied multiple
908 times to different values of the response or outcome variable, such as the effect estimates at the voxels within the brain.
909 As the conventional voxel-wise neuroimaging data analysis is performed with a massively univariate approach, there are
910 as many models as the number of voxels, which is the source of the major multiplicity issue: multiple testing. Those
911 models can be, for instance, Student’s t -tests, AN(C)OVA, univariate or multivariate GLM, LME or Bayesian model.
912 Regardless of the specific model, all the voxels share the same design matrix, but have different response variable values on
913 the left-hand side of the equation. With human brain size on the order of 10^6 mm³, the number of voxels may range from
914 20,000 to 150,000 depending on the voxel dimensions. Each extra voxel adds an extra model and leads to incrementally
915 mounting odds of pure chance or “statistically significant outcomes,” presenting the challenge to account for the occurrence
916 of mounting family-wise error (FWE), while effectively holding the overall false positive rate (FPR) at a nominal level
917 (e.g., 0.05). In the same vein, surface-based analysis is performed with 30,000 to 50,000 nodes (Saad et al., 2004), sharing a
918 similar multiple testing issue with its volume-based counterpart. Sometimes the investigator performs analyses at smaller

$ef \backslash se$	0.1			0.3			0.5			0.7			1.0		
	pwr	S	M	pwr	S	M	pwr	S	M	pwr	S	M	pwr	S	M
0.1	0.15	0.02	2.66	0.06	0.21	7.58	0.05	0.31	12.86	0.05	0.36	17.71	0.05	0.40	25.55
0.3	0.81	0.00	1.12	0.15	0.02	2.66	0.08	0.09	4.28	0.07	0.15	5.96	0.06	0.23	8.59
0.5	1.00	0.00	1.00	0.34	0.00	1.67	0.15	0.02	2.66	0.10	0.06	3.66	0.07	0.12	5.16
0.7	1.00	0.00	1.00	0.60	0.00	1.28	0.25	0.00	1.96	0.15	0.02	2.67	0.10	0.06	3.74
1.0	1.00	0.00	1.00	0.89	0.00	1.07	0.47	0.00	1.44	0.26	0.00	1.91	0.15	0.02	2.65

The simulations were performed using a modified version of the code from Gelman and Carlin (2014). The power (pwr , gray column), type S (S , white column) and type M (M , cyan column) errors are estimated using 10,000 iterations with a Student's $t(20)$ -distribution for an FMRI population analysis. The setup parameters of each simulation were the true effect (ef) and standard error (se), which are provided in the row and column labels, respectively. The true effect and standard error values ranged from 0.1-1.0, representing units of percent signal change. The combination (in purple) with effect of 0.3% and standard error of 1.0% is used to illustrate the various types of errors further in Fig. 5. In each simulation, the power is estimated as the sum of the two tailed areas beyond the threshold at the standard significance level of 0.05 (shown in blue in Fig. 5). Type S error is the ratio of the tailed area that has the opposite sign of the true effect relative to power, and type M error is expressed as the average value of “significant” results across all simulations relative to the true effect. In the lower triangle, effects with high power ($pwr \approx 1$) tend to have low type S error ($S \approx 0$) and low type M error ($M \approx 1$). However, as power decreases, type S error increases to a large fraction of unity, and $M \gg 1$.



The simulation results in the above table are illustrated as three separate plots below, respectively, for power, type S and type M errors. The combination (purple in the table) with effect of 0.3% and standard error of 1.0% is shown with the large purple diamond in the plots. Substantial type S and type M errors occur when the true effect is low and unreliable (i.e., with high standard error), shown here especially at the left side of the black and green curves.

Figure 4: Power, type S and type M errors estimated from simulations

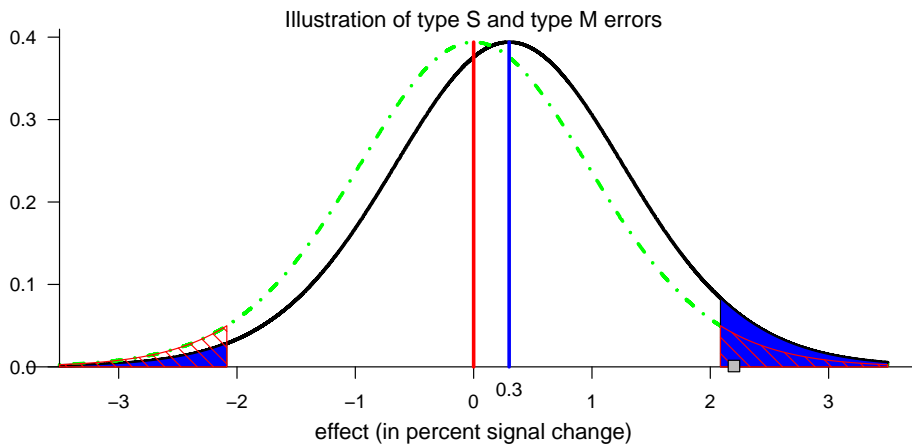


Figure 5: Illustration of the concept and interpretation for power, type I, type S and type M errors (Gelman, 2015). Suppose that there is a hypothetical Student's $t(20)$ -distribution (black curve) for a true effect (blue vertical line) of 0.3 and a corresponding standard error of 1.0 percent signal change, a scenario highlighted in purple in Fig. 4. Under the null hypothesis (red vertical line and dot-dashed green curve), two-tailed testing with a type I error rate of 0.05 leads to having thresholds at ± 2.086 ; FPR = 0.05 corresponds to the null distribution's total area beyond these two critical values (marked with red diagonal lines). The power is the total area of the $t(20)$ -distribution for the true effect (black curve) beyond these thresholds, which is 0.06 (shaded in blue). The type S error is the ratio of the blue area in the true effect distribution's left tail beyond the threshold of -2.086 to the area in both tails, which is 23% here (i.e., the ratio of the “significant” area in the wrong-signed tail to that of the total “significant” area). If a random draw from the $t(20)$ -distribution under the true effect happens to be 2.2 (small gray square), it would be identified as statistically significant at the 0.05 level, and the resulting type M error would quantify the magnification of the estimated effect size as $2.2/0.3 \approx 7.33$, which is much larger than unity.

919 number of regions of interest (ROIs), perhaps of order 100, but even here adjustment is still required for the multiple
920 testing issue (though it is often not made).

921 B) *Double sidedness*. Another occurrence of multiplicity is the widespread adoption of two separate one-sided (or
922 one-tailed) tests in neuroimaging. For instance, the comparison between the two conditions of “easy” and “difficult” are
923 usually analyzed twice for the whole brain: one showing whether the easy effect is higher than difficult, and the other for
924 the possibility of the difficult effect being higher than easy. One-sided testing for one direction would be justified if prior
925 knowledge is available regarding the sign of the test for a particular brain region. When no prior information is available for
926 all regions in the brain, one cannot simply finesse two separate one-sided tests in place of one two-sided test, and a double
927 sidedness practice warrants a Bonferroni correction because the two tails are independent with respect to each other (and
928 each one-sided test is more liberal than a two-sided test at the same significance level). However, simultaneously testing
929 both tails in tandem for whole brain analysis without correction is widely used without clear justification, and this forms
930 a source of multiplicity issue that needs proper accounting (Chen et al., 2018).

931 C) *Multiple comparisons*. It rarely occurs that only one statistical test is carried out in a specific neuroimaging study,
932 such as a single one-sample t -test. Therefore, a third source of multiplicity is directly related to the popular term, multiple
933 comparisons, which occur when multiple tests are conducted under one model. For example, an investigator that designs
934 an emotion experiment with three conditions (easy, difficult, and moderate) may perform several separate tests: comparing
935 each of the three conditions to baseline, making three pairwise comparisons, or testing a linear combination of the three
936 conditions (such as the average of easy and difficult versus moderate). However, neuroimaging publications seldom consider
937 corrections for such separate tests.

938 D) *Multiple paths*. The fourth multiplicity issue to affect outcome interpretation arises from the number of potential
939 preprocessing, data dredging and analytical pipelines (Carp, 2012). For instance, all common steps have a choice of
940 procedures: outlier handling (despiking, censoring), slice timing correction (yes/no, various interpolations), head motion
941 correction (different interpolations), different alignment methods from EPI to anatomical data plus upsampling (1 to 4
942 mm), different alignment methods to different standard spaces (Talairach and MNI variants), spatial smoothing (3 to 10
943 mm), data scaling (voxel-wise, global or grand mean), confounding effects (slow drift modeling with polynomials, high
944 pass filtering, head motion parameters), hemodynamic response modeling (different presumed functions and multiple basis
945 functions), serial correlation modeling (whole brain, tissue-based, voxel-wise AR or ARMA), and population modeling
946 (univariate or multivariate GLM, treating sex as a covariate of no interest (thus no interactions with other variables) or as
947 a typical factor (plus potential interactions with other variables)). Each choice represents a “branching point” that could
948 have a quantitative change to the final effect estimate and inference. Conservatively assuming three options at each step
949 here would yield totally $3^{10} = 59,049$ possible paths, commonly referred to as researcher degrees of freedom (Simmons
950 et al., 2011). The impact of the choice at each individual step for this abbreviated list might be negligible, moderate, or
951 substantial. For example, different serial correlation models may lead to substantially different effect estimate reliability
952 (Olszowy et al., 2017); the estimate for spatial correlation of the noise could be sensitive to the voxel size to which the
953 original data were upsampled (Mueller et al., 2017; Cox and Taylor, 2017), which may lead to different cluster thresholds
954 and poor control to the intended FPR in correcting for multiplicity. Therefore, the cumulative effect across all these
955 multilevel branching points could be a large divergence between any two paths for the final results. A multiverse analysis
956 (Steenen et al., 2016) has been suggested for such situations of having a “garden of forking paths” (Gelman and Loken,
957 2013), but this seems highly impractical for neuroimaging data. Even when one specific analytical path is chosen by the
958 investigator, it remains possible to invoke potential or implicit multiplicity in the sense that the details of the analytical
959 steps such as data sanitation are conditional on the data (Gelman and Loken, 2013). The final interpretation of significance
960 typically ignores the number of choices or the potential branchings that may affect the final outcome, even though it would
961 be more preferable to have the statistical significance independent of these preprocessing steps.

962 Appendix D. Bayesian modeling for one-way random-effects ANOVA

Here we discuss a classical framework, a hierarchical or multilevel model for a one-way random-effects ANOVA, and use it as a building block to expand to a Bayesian framework for neuroimaging group analysis. In evaluating this model, the controllability of inference errors will be focused on type S errors instead of the traditional FPR. Suppose that there are r measured entities (e.g., ROIs), with entity j measuring the effect θ_j from n_j independent Gaussian-distributed data points y_{ij} , each of which represents a sample (e.g., trial), $i = 1, 2, \dots, n_j$. The conventional statistical approach formulates

r separate models,

$$y_{ij} = \theta_j + \epsilon_{ij}, \quad i = 1, 2, \dots, n_j, \quad (18)$$

where ϵ_{ij} is the residual for the j th entity and is assumed to be Gaussian $\mathcal{N}(0, \sigma^2)$, $j = 1, 2, \dots, r$. Depending on whether the sampling variance σ^2 is known or not, each effect can be assessed through its sample mean $\bar{y}_{\cdot j} = \frac{1}{n_j} \sum_{i=1}^{n_j} y_{ij}$ relative to the corresponding variance $V_j^0 = \frac{\sigma^2}{n_j}$, resulting in a Z - or t -test.

By combining the data from the r entities and further decomposing the effect θ_j into an overall effect b_0 across the r entities and the deviation ξ_j of the j th entity from the overall effect (i.e., $\theta_j = b_0 + \xi_j, j = 1, 2, \dots, r$), we have a conventional one-way random-effects ANOVA,

$$y_{ij} = b_0 + \xi_j + \epsilon_{ij}, \quad i = 1, 2, \dots, n_j, \quad j = 1, 2, \dots, r, \quad (19)$$

where b_0 is conceptualized as a fixed-effects parameter, ξ_j codes the random fluctuation of the j th entity from the overall mean b_0 , with the assumption of $\xi_j \sim \mathcal{N}(0, \tau^2)$, and the residual ϵ_{ij} follows a Gaussian distribution $\mathcal{N}(0, \sigma^2)$. The classical one-way random-effects ANOVA model (19) is typically formulated to examine the null hypothesis,

$$H_0 : \tau = 0, \quad (20)$$

with an F -statistic, which is constructed as the ratio of the *between* mean sums of squares and the *within* mean sums of squares. An application of this ANOVA model (19) to neuroimaging is to compute the intraclass correlation ICC(1,1) as $\frac{\tau^2}{\tau^2 + \sigma^2}$ when the measuring entities are exchangeable (e.g., families with identical twins; Chen et al., 2017c).

Whenever multiple values (e.g., two effect estimates from two scanning sessions) from each measuring unit (e.g., subject or family) are correlated (e.g., the levels of a within-subject or repeated-measures factor), the data can be formulated using a linear mixed-effects (LME) model, sometimes referred to as a multilevel or hierarchical model. One natural ANOVA extension is simply to treat the model conceptually as LME, without the need of reformulating the model equation (19). However, LME can only provide point estimates for the overall effect b_0 , cross-region variance τ^2 and the data variance σ^2 ; that is, the LME (19) cannot directly provide any information regarding the individual ξ_j or θ_j values because of over-fitting due to the fact that the number of data points is less than the number of parameters that need to be estimated.

Our interest here is neither to assess the variability τ^2 nor to calculate ICC, but instead to make statistical inferences about the individual effects θ_j . Nevertheless, the conventional NHST (20) may shed some light on potential strategies (Gelman et al., 2014) for θ_j . If the deviations ξ_j are relatively small compared to the overall mean b_0 , then the corresponding F -statistic value will be small as well, leading to the decision of not rejecting the null hypothesis (20) at a reasonable, predetermined significance level (e.g., 0.05); in that case, we can estimate the equal individual effects θ_j using the overall weighted mean \bar{y}_{\cdot} through full pooling with all the data,

$$\hat{\theta}_1 = \hat{\theta}_2 = \dots = \hat{\theta}_r = \bar{y}_{\cdot} = \frac{\sum_{j=1}^r \frac{1}{\sigma_j^2} \bar{y}_{\cdot j}}{\sum_{j=1}^r \frac{1}{\sigma_j^2}}, \quad (21)$$

where $\bar{y}_{\cdot j} = \frac{1}{n_j} \sum_{i=1}^{n_j} y_{ij}$ and $\sigma_j^2 = \frac{\sigma^2}{n_j}$ are the sampling mean and variance for the j th measuring entity, and the subscript dot (\cdot) notation indicates the (weighted) mean across the corresponding index(es). On the other hand, if the deviations ξ_j are relatively large, so is the associated F -statistic value, leading to the decision of rejecting the null hypothesis (20); similarly, we can reasonably estimate θ_j with no pooling across the r entities; that is, each θ_j is estimated using the j th measuring entity's data separately,

$$\hat{\theta}_j = \bar{y}_{\cdot j} = \frac{1}{n_j} \sum_{i=1}^{n_j} y_{ij}, \quad j = 1, 2, \dots, r. \quad (22)$$

However, in estimating θ_j we do not have to take a dichotomous approach of choosing, based on a preset significance level, between these two extreme choices, the overall weighted mean \bar{y}_{\cdot} in (21) through full pooling and the separate means $\bar{y}_{\cdot j}$ in (22) with no pooling; instead, we could make the assumption that a reasonable estimate to θ_j lies somewhere along the continuum between \bar{y}_{\cdot} and $\bar{y}_{\cdot j}$, with its exact location derived from the data instead of by imposing an arbitrary threshold. This thinking brings us to the Bayesian methodology.

To simplify the situation, we first assume a known sampling variance σ^2 for the i th data point (e.g., trial) for the j th entity; or, in Bayesian-style formulation, we build a BML about the distribution of y_{ij} conditional on θ_j ,

$$y_{ij}|\theta_j \sim \mathcal{N}(\theta_j, \sigma^2), \quad i = 1, 2, \dots, n_j, \quad j = 1, 2, \dots, r. \quad (23)$$

With a prior distribution $\mathcal{N}(b_0, \tau^2)$ for θ_j and a noninformative uniform hyperprior for b_0 given τ (i.e., $b_0|\tau \sim 1$), the conditional posterior distributions for θ_j can be derived (Gelman et al., 2014) as,

$$\theta_j|b_0, \tau, y \sim \mathcal{N}(\hat{\theta}_j, V_j), \quad \text{where } \hat{\theta}_j = \frac{\frac{1}{\sigma_j^2}\bar{y}_{\cdot j} + \frac{1}{\tau^2}b_0}{\frac{1}{\sigma_j^2} + \frac{1}{\tau^2}}, \quad V_j = \frac{1}{\frac{1}{\sigma_j^2} + \frac{1}{\tau^2}}, \quad \sigma_j^2 = \frac{\sigma^2}{n_j}, \quad j = 1, 2, \dots, r. \quad (24)$$

The analytical solution (24) indicates that $\frac{1}{V_j} = \frac{1}{\sigma_j^2} + \frac{1}{\tau^2}$, manifesting an intuitive fact that the posterior precision is the cumulative effect of the data precision and the prior precision; that is, the posterior precision is improved by the amount $\frac{1}{\tau^2}$ relative to the data precision $\frac{1}{\sigma_j^2}$. Moreover, the expression for the posterior mode of $\hat{\theta}_j$ in (24) shows that the estimating choice in the continuum can be expressed as a precision-weighted average between the individual sample means $\bar{y}_{\cdot j}$ and the overall mean b_0 :

$$\hat{\theta}_j = \frac{\frac{1}{\sigma_j^2}\bar{y}_{\cdot j} + \frac{1}{\tau^2}b_0}{\frac{1}{\sigma_j^2} + \frac{1}{\tau^2}} = w_j\bar{y}_{\cdot j} + (1 - w_j)b_0 = b_0 + w_j(\bar{y}_{\cdot j} - b_0) = \bar{y}_{\cdot j} - (1 - w_j)(\bar{y}_{\cdot j} - b_0), \quad j = 1, 2, \dots, r, \quad (25)$$

where the weights $w_j = \frac{V_j}{\sigma_j^2}$. The precision weighting in (25) makes intuitive sense in terms of the previously described limiting cases:

- i. The full pooling (21) corresponds to $w_j = 0$ or $\tau^2 = 0$, which means that the θ_j are assumed to be the same or fixed at a common value. The approach would lead to underfitting because the effect is assumed to be invariance across ROIs.
- ii. The no pooling (22) corresponds to $w_j = 1$ or $\tau^2 = \infty$, indicating that the r effects θ_j are uniformly distributed within $(-\infty, \infty)$; that is, it corresponds to a noninformative uniform prior on θ_j . In contrast to full pooling, no pooling tends to overfit the data as the information at one ROI is not utilized to shed light on any other ROIs.
- iii. The partial pooling (24) or (25) reflects the fact that the r effects θ_j are *a priori* assumed to follow an independent and identically distribution, the prior $\mathcal{N}(b_0, \tau^2)$. Under the Bayesian framework, we make statistical inferences about the r effects θ_j with a posterior distribution (24) that includes the conventional dichotomous decisions between full pooling (21) and no pooling (22) as two special and extreme cases. Moreover, as expressed in (25), the Bayesian estimate $\hat{\theta}_j$ can be conceptualized as the precision-weighted average between the individual estimate $\bar{y}_{\cdot j}$ and the overall (or prior) mean b_0 , the adjustment of θ_j from the overall mean b_0 toward the observed mean $\bar{y}_{\cdot j}$, or conversely, the observed mean $\bar{y}_{\cdot j}$ being shrunk toward the overall mean b_0 . As a middle ground between full pooling and no pooling, partial pooling usually provides a better fit to the data since the information is effectively pooled and shared across ROIs.

An important concept for a Bayesian model is exchangeability. Specifically for the BML (23), the effects θ_j are exchangeable if their joint distribution $p(\theta_1, \theta_2, \dots, \theta_r)$ is immutable or invariant to any random permutation among their indices or orders (e.g., $p(\theta_1, \theta_2, \dots, \theta_r)$ is a symmetric function). Using the ROIs as an example, exchangeability means that, without any *a priori* knowledge about their effects, we can randomly shuffle or relabel them without reducing our knowledge about their effects. In other words, complete ignorance equals exchangeability: before poring over the data, there is no way for us to distinguish the regions from each other. When the exchangeability assumption can be assumed for θ_j , their joint distribution can be expressed as a mixture of independent and identical distributions (Gelman et al., 2014), which is essential in the derivation of the posterior distribution (24) from the prior distribution $\mathcal{N}(b_0, \tau^2)$ for θ_j .

To complete the Bayesian inferences for the model (23), we proceed to obtain (i) $p(b_0, \tau|y)$, the marginal posterior distribution of the hyperparameters (b_0, τ) , (ii) $p(b_0|\tau, y)$, the posterior distribution of b_0 given τ , and (iii) $p(\tau|y)$, the posterior distribution of τ with a prior for τ , for example, a noninformative uniform distribution $p(\tau) \sim 1$. In practice, the numerical solutions are achieved in a backward order, through Monte Carlo simulations of τ to get $p(\tau|y)$, simulations of b_0 to get $p(b_0|\tau, y)$, and, lastly, simulations of θ_j to get $p(\theta_j|b_0, \tau, y)$ in (24).

Assessing type S error under BML

In addition to the advantage of information merging across the r entities between the limits of complete and no pooling, a natural question remains: how does BML perform in terms of the conventional type I error as well as type S and type M errors? With the “standard” analysis of r separate models in (18), each effect θ_j is assessed against the sampling variance $V_j^0 = \sigma_j^2$. In contrast, under the BML (23), the posterior variance, as shown in (24), is $V_j = \frac{1}{\frac{1}{\sigma_j^2} + \frac{1}{\tau^2}}$, $\sigma_j^2 = \frac{\sigma^2}{n_j}$. As the ratio of the two variances $\frac{V_j^0}{V_j} = \frac{\tau^2}{\tau^2 + \sigma_j^2}$ is always less than 1 (except for the limiting cases of $\sigma^2 \rightarrow 0$ or $\tau^2 \rightarrow \infty$), BML generally assigns a larger uncertainty than the conventional approach with no pooling. That is, the inference for each effect θ_j based on the unified model (23) is more conservative than when the effect is assessed individually through the model (18). Instead of tightening the overall FPR through some kind of correction for multiplicity among the r separate models, BML addresses the multiplicity issue through precision adjustment or partial pooling under one model with a shrinking or pooling strength of $\sqrt{\frac{V_j^0}{V_j}} = \frac{1}{\sqrt{1 + \sigma_j^2/\tau^2}}$.

Simulations (Gelman and Tuerlinckx, 2000) indicate that, when making inference based on the 95% quantile interval of the posterior distribution for a single effect θ_j (j is fixed, e.g., $j = 1$), the type S error rate for the Bayesian model (23) is less than 0.025 under all circumstances. In contrast, the conventional model (18) would have a substantial type S error rate especially when the sampling variance is large relative to the cross-entities variance (e.g., $\sigma_j^2/\tau^2 > 2$); specifically, type S error reaches 10% when $\sigma_j^2/\tau^2 = 2$, and may go up to 50% if σ_j^2 much larger than τ^2 . When multiple comparisons are performed, a similar patterns remains; that is, the type S error rate for the Bayesian model is in general below 2.5%, and is lower than the conventional model with rigorous correction (e.g., Tukey’s honestly significant difference test, wholly significant differences) for multiplicity when $\sigma/\tau > 1$. The controllability of BML on type S errors is parallel to the usual focus on type I errors under NHST; however, unlike NHST in which the typical I error rate is deliberately controlled through a an FPR threshold, the controllability of type S errors under BML is intrinsically embedded in the modeling mechanism without any explicit imposition.

The model (23) is typically seen in Bayesian statistics textbooks as an intuitive introduction to BML (e.g., Gelman et al., 2014). With the indices i and j coding the task trials and ROIs, respectively, the ANOVA model (19) or its Bayesian counterpart (23) can be utilized to make inferences on an ensemble of ROIs at the individual subject level. The conventional analysis would have to deal with the multiplicity issue because of separate inferences at each ROI (i.e., entity). In contrast, there is only one integrated model (23) that leverages the information among the r entities, and the resulting partial pooling effectively dissolves the multiple testing concern. However, the modeling framework can only be applied for single subject analysis, and it is not suitable at the population level; nevertheless, it serves as an intuitive tool for us to extend to more sophisticated scenarios.

Appendix E. Derivation of posterior distribution for BML (5)

We start with the BML system (5) with a known sampling variance σ^2 ,

$$y_{ij}|\pi_i, \theta_j \sim \mathcal{N}(\pi_i + \theta_j, \sigma^2), \quad i = 1, 2, \dots, n, \quad j = 1, 2, \dots, r.$$

Conditional on θ_j and prior $\pi_i \sim N(0, \lambda^2)$, the variance for the sampling mean at the j th ROI, $\bar{y}_{\cdot j} = \frac{1}{n} \sum_{i=1}^n y_{ij} = \theta_j + \frac{1}{n} \sum_{i=1}^n \pi_i + \frac{1}{n} \sum_{i=1}^n \epsilon_{ij}$, is $\frac{\lambda^2 + \sigma^2}{n}$; that is,

$$\bar{y}_{\cdot j}|\theta_j, \lambda^2 \sim N\left(\theta_j, \frac{\lambda^2 + \sigma^2}{n}\right), \quad j = 1, 2, \dots, r.$$

With priors $\pi_i \sim N(0, \lambda^2)$ and $\theta_j \sim N(\mu, \tau^2)$, we follow the same derivation as in the likelihood (23), and obtain the posterior distribution,

$$\theta_j|\mu, \tau, \lambda, \mathbf{y} \sim \mathcal{N}(\hat{\theta}_j, V), \quad \text{where } \mathbf{y} = \{y_{ij}\}, \hat{\theta}_j = \frac{\frac{n}{\lambda^2 + \sigma^2} \bar{y}_{\cdot j} + \frac{1}{\tau^2} \mu}{\frac{n}{\lambda^2 + \sigma^2} + \frac{1}{\tau^2}}, \quad V = \frac{1}{\frac{n}{\lambda^2 + \sigma^2} + \frac{1}{\tau^2}}, \quad j = 1, 2, \dots, r.$$

When the sampling variance σ^2 is unknown, we can solve the LME counterpart in (4),

$$y_{ij} = \mu + \pi_i + \xi_j + \epsilon_{ij}, \quad i = 1, 2, \dots, n, \quad j = 1, 2, \dots, r.$$

1042 We then plug the estimated variances $\hat{\lambda}^2$, $\hat{\tau}^2$ and $\hat{\sigma}^2$ into the above posterior distribution formulas, and obtain the posterior
1043 mean and variance through an approximate Bayesian approach.

1044 References

- 1045 Amrhein, V., Greenland, S., 2017. Remove, rather than redefine, statistical significance. *Nature Hum. Behav.* 1:0224.
- 1046 Bates, B., Maechler, M., Bolker, B. Walker, S. 2015. Fitting Linear Mixed-Effects Models Using lme4. *Journal of*
1047 *Statistical Software*, 67(1):1-48.
- 1048 Benjamin, D. J., Berger, J., Johannesson, M., Nosek, B. A., Wagenmakers, E.-J., Berk, R., \acute{E} , Johnson, V., 2017.
1049 Redefine statistical significance. *Nature Hum. Behav.* 1:0189.
- 1050 Benjamini, Y., Hochberg, Y., 1995. Controlling the false discovery rate: a practical and powerful approach to multiple
1051 testing. *Journal of the Royal Statistical Society Series B* 57, 289-300.
- 1052 Carp, J., 2012. On the Plurality of (Methodological) Worlds: Estimating the Analytic Flexibility of fMRI Experiments.
1053 *Frontiers in Neuroscience* 6:149.
- 1054 Chen, G., Saad, Z.S., Nath, A.R., Beauchamp, M.S., Cox, R.W., 2012. FMRI Group Analysis Combining Effect
1055 Estimates and Their Variances. *NeuroImage* 60:747-765.
- 1056 Chen, G., Saad, Z.S., Britton, J.C., Pine, D.S., Cox, R.W., 2013. Linear Mixed-Effects Modeling Approach to FMRI
1057 Group Analysis. *NeuroImage* 73:176-190.
- 1058 Chen, G., Adleman, N.E., Saad, Z.S., Leibenluft, E., Cox, R.W., 2014. Applications of Multivariate Modeling to
1059 Neuroimaging Group Analysis: A Comprehensive Alternative to Univariate General Linear Model. *NeuroImage* 99, 571-
1060 588.
- 1061 Chen, G., Saad, Z.S., Adleman, N.E., Leibenluft, E., Cox, R.W., 2015. Detecting the subtle shape differences in
1062 hemodynamic responses at the group level. *Front. Neurosci.* 9: 375.
- 1063 Chen, G., Taylor, P.A., Shin, Y.W., Reynolds, R.C., Cox, R.W., 2017a. Untangling the Relatedness among Correlations,
1064 Part II: Inter-Subject Correlation Group Analysis through Linear Mixed-Effects Modeling. *Neuroimage* 147:825-840.
- 1065 Chen, G., Taylor, P.A., Cox, R.W., 2017b. Is the statistic value all we should care about in neuroimaging? *Neuroimage*
1066 147:952-959.
- 1067 Chen, G., Taylor, P.A., Haller, S.P., Kircanski, K., Stoddard, J., Pine, D.S., Leibenluft, E., Brotman, M.A., Cox, R.W.,
1068 2017c. Intraclass correlation: improved modeling approaches and applications for neuroimaging. *Human Brain Mapping*.
1069 *Human Brain Mapping*. DOI: 10.1002/hbm.23909
- 1070 Chen, G., Cox, R.W., Glen, D.R., Rajendra, J.K., Reynolds, R.C., Taylor, P.A., 2018. A tail of two sides: Artificially
1071 doubled false positive rates in neuroimaging due to the sidedness choice with t-tests. *Human Brain Mapping*. In press.
- 1072 Cohen, J., 1994. The earth is round ($p < .05$). *American Psychologist* 49(12):997-1003.
- 1073 Cox, R.W., 1996. AFNI: software for analysis and visualization of functional magnetic resonance neuroimages. *Comput.*
1074 *Biomed. Res.* 29:162-173. <http://afni.nimh.nih.gov>.
- 1075 Cox, R.W., Chen, G., Glen, D.R., Reynolds, R.C., Taylor, P.A., 2017. FMRI Clustering in AFNI: False-Positive Rates
1076 Redux. *Brain Connect.* 7(3):152-171.
- 1077 Cox, R.W., 2018. Equitable Thresholding and Clustering. In preparation.
- 1078 Cox, R.W., Taylor, P.A., 2017. Stability of Spatial Smoothness and Cluster-Size Threshold Estimates in FMRI using
1079 AFNI. <https://arxiv.org/abs/1709.07471>
- 1080 Cremers, H.R., Wager, T.D., Yarkoni, T., 2017. The Relation Between Statistical Power and Inference in fMRI. *PLoS*
1081 *ONE* 12(11):e0184923
- 1082 Eklund, A., Nichols, T.E., Knutsson, H., 2016. Cluster failure: Why fMRI inferences for spatial extent have inflated
1083 false-positive rates. *PNAS* 113(28):7900-7905.
- 1084 Forman, S.D., Cohen, J.D., Fitzgerald, M., Eddy, W.F., Mintun, M.A., Noll, D.C., 1995. Improved assessment of
1085 significant activation in functional magnetic resonance imaging (fMRI): use of a cluster-size threshold. *Magn Reson Med*.
1086 33:636-647.
- 1087 Gelman, A., 2015. Statistics and the crisis of scientific replication. *Significance* 12(3):23-25.
- 1088 Gelman, A., 2016. The problems with p -values are not just with p -values. *The American Statistician*, Online Discussion.
- 1089 Gelman, A., Carlin, J.B., 2014. Beyond Power Calculations: Assessing Type S (Sign) and Type M (Magnitude) Errors.
1090 *Perspectives on Psychological Science* 1-11.

1091 Gelman, A., Carlin, J.B., Stern, H.S., Dunson, D.B., Vehtari, A., Rubin, D.B., 2014. Bayesian data analysis. Third
1092 edition. Chapman & Hall/CRC Press.

1093 Gelman, A., Hennig, C., 2016. Beyond subjective and objective in statistics.
1094 <http://www.stat.columbia.edu/~gelman/research/unpublished/objectivityr3.pdf>

1095 Gelman, A., Hill, J. Yajima, M., 2012. Why we (usually) don't have to worry about multiple comparisons. *Journal of*
1096 *Research on Educational Effectiveness* 5:189-211.

1097 Gelman, A., Loken, E., 2013. The garden of forking paths: Why multiple comparisons can be a problem, even when
1098 there is no "fishing expedition" or "p-hacking" and the research hypothesis was posited ahead of time.
1099 http://www.stat.columbia.edu/~gelman/research/unpublished/p_hacking.pdf

1100 Gelman, A., Shalizi, C.R., 2013. Philosophy and the practice of Bayesian statistics. *British Journal of Mathematical*
1101 *and Statistical Psychology* 66:8-38.

1102 Gelman, A., Simpson, D., Betancourt, M., 2017. The prior can generally only be understood in the context of the
1103 likelihood. arXiv:1708.07487

1104 Gelman, A., Tuerlinckx, F., 2000. Type S error rates for classical and Bayesian single and multiple comparison
1105 procedures. *Computational Statistics* 15: 373-390.

1106 Gonzalez-Castillo, J., Saad, Z.S., Handwerker, D.A., Inati, S.J., Brenowitz, N., Bandettini, P.A., 2012. Whole-brain,
1107 time-locked activation with simple tasks revealed using massive averaging and model-free analysis. *PNAS* 109 (14), 5487-
1108 5492.

1109 Gonzalez-Castillo, J., Chen, G., Nichols, T., Cox, R.W., 2017. Bandettini, P.A., Variance Decomposition for Single-
1110 Subject task-based fMRI activity estimates across many sessions. *NeuroImage* 154:206-218.

1111 Lazzeroni, L.C., Lu, Y., Belitskaya-Lévy, I., 2016. Solutions for quantifying P-value uncertainty and replication power.
1112 *Nature Methods* 13:107-110.

1113 Lewandowski, D., Kurowicka, D., Joe, H., 2009. Generating random correlation matrices based on vines and extended
1114 onion method. *Journal of Multivariate Analysis*, 100, 1989-2001.

1115 Loken E., Gelman, A., 2017. Measurement error and the replication crisis. *Science* 355(6325):584-585.

1116 McElreath R., 2016, *Statistical Rethinking: A Bayesian Course with Examples in R and Stan*. Chapman & Hall/CRC
1117 Press.

1118 McShane, B.B., Gal, D., Gelman, A., Robert, C., Tackett, J.L., 2017. Abandon Statistical Significance. arXiv:1709.07588

1119 Mejia, A., Yue, Y.R., Bolin, D., Lindren, F., Lindquist, M.A., 2017. A Bayesian General Linear Modeling Approach to
1120 Cortical Surface fMRI Data Analysis. arXiv:1706.00959

1121 Morey, R.D., Hoekstra, R., Rouder, J.N., Lee, M.D., Wagenmakers, E.-J., 2016. The fallacy of placing confidence in
1122 confidence intervals. *Psychonomic Bulletin and Review* 23(1):103-123.

1123 Mueller, K., Lepsien, J., Möller, H.E., Lohmann, G., 2017. Commentary: Cluster failure: Why fMRI inferences for
1124 spatial extent have inflated false-positive rates. *Front Hum Neurosci* 11:345.

1125 Nichols, T.E., Holmes, A.P., 2001. Nonparametric permutation tests for functional neuroimaging: a primer with
1126 examples. *Hum Brain Mapp.* 15(1):1-25.

1127 Olszowy, W., Aston, J., Rua, C., Williams, G.B., 2017. Accurate autocorrelation modeling substantially improves fMRI
1128 reliability. arXiv:1711.09877

1129 Poline, J.B., Brett, M., 2012. The general linear model and fMRI: does love last forever? *Neuroimage* 62(2):871-880.

1130 R Core Team, 2017. R: A language and environment for statistical computing. R Foundation for Statistical Computing,
1131 Vienna, Austria. <https://www.R-project.org/>

1132 Saad, Z.S., Reynolds, R.C., Argall, B., Japee, S., Cox, R.W., 2004. SUMA: An interface for surface-based intra- and
1133 inter-subject analysis with AFNI. *Proc. 2004 IEEE International Symposium on Biomedical Imaging*, 1510-1513.

1134 Schaefer, A., Kong, R., Gordon, E.M., Zuo, X.N., Holmes, A.J., Eickhoff, S.B., Yeo, B.T., 2017. Local-global parcellation
1135 of the human cerebral cortex from intrinsic functional connectivity MRI. *Cerebral Cortex*. In press.

1136 Simmons, J. P., Nelson, L. D., Simonsohn, U., 2011. False-positive psychology: Undisclosed flexibility in data collection
1137 and analysis allows presenting anything as significant. *Psychological Science* 22:1359-1366.

1138 Smith, S.M., Nichols, T.E., 2009. Threshold-free cluster enhancement: addressing problems of smoothing, threshold
1139 dependence and localisation in cluster inference. *Neuroimage*. 44(1):83-98.

1140 Stan Development Team, 2017. Stan Modeling Language Users Guide and Reference Manual, Version 2.17.0. [http://mc-](http://mc-stan.org)
1141 [stan.org](http://mc-stan.org)

1142 Steegen, S., Tuerlinckx, F., Gelman, A., Vanpaemel, W., 2016. Increasing transparency through a multiverse Analysis.
1143 *Perspect Psychol Sci.*11(5):702-712.

1144 Wasserstein, R.L., Lazar, N.A., 2016. The ASA's statement on p -values: context, process, and purpose. *The American*
1145 *Statistician* 70:2, 129-133.

1146 Vehtari, A., Gelman, A. Gabry, J., 2017. Practical Bayesian model evaluation using leave-one-out cross-validation and
1147 WAIC. *Statistics and Computing* 27(5):1413-1432.

1148 Westfall, J., Nichols, T.E., Yarkoni, T., 2017. Fixing the stimulus-as-fixed-effect fallacy in task fMRI. *Wellcome Open*
1149 *Research* 1:23.

1150 Wickham, H., 2009. *ggplot2: Elegant Graphics for Data Analysis*. Springer-Verlag, New York.

1151 Worsley, K.J., Marrett, S., Neelin, P., Evans, A.C., 1992. A three-dimensional statistical analysis for CBF activation
1152 studies in human brain. *Journal of Cerebral Blood Flow and Metabolism*, 12:900-918.

1153 Xiao, Y., Geng, F., Riggins, T., Chen, G., Redcay, E., 2018. Neural correlates of developing theory of mind competence
1154 in early childhood. Under review.

1155 Yeung, A.W.K., 2018. An updated survey on statistical thresholding and sample size of fMRI studies. *Front Hum*
1156 *Neurosci.* 12:16.